IEEE Access
Multidisciplinary ⋮ Rapid Review ⋮ Open Access Journal

Received 1 October 2025, accepted 17 October 2025, date of publication 23 October 2025, date of current version 30 October 2025.

Digital Object Identifier 10.1109/ACCESS.2025.3624655

TOPICAL REVIEW

Advances in Metantennas: Classification and Future Prospects

MD ASHIF ISLAM ONI[1], (Graduate Student Member, IEEE), YANG YANG[2], (Senior Member, IEEE), AND SHUVASHIS DEY[1], (Member, IEEE)

[1]Department of Electrical and Computer Engineering, North Dakota State University, Fargo, ND 58105, USA
[2]School of Electrical and Data Engineering, University of Technology Sydney, Ultimo, Sydney, NSW 2007, Australia

Corresponding author: Shuvashis Dey (shuvashis.dey@ndsu.edu)

This work was supported in part by U.S. Department of Agriculture (USDA) Agricultural Research Service (ARS) under Grant FAR0037087.

ABSTRACT Metamaterials are three-dimensional engineered structures that manipulate electromagnetic waves in bulk, while Metasurfaces are their two-dimensional counterparts, enabling wave control with reduced thickness and simpler fabrication. These technologies have revolutionized antenna design, enabling the development of advanced metasurface antennas (metantennas) with unprecedented electromagnetic wave control. This article comprehensively reviews the classification, advancements, and prospects of metantennas, emphasizing applications in 5G and beyond. Metantennas, which use metasurfaces as primary radiating apertures, achieve significant improvements in key performance metrics. The review categorizes electromagnetic metasurfaces by operation, generation, and function, and analyzes various metantenna types with their design principles, advantages, challenges, and applications. It also highlights the impact of emerging materials and technologies on metantenna evolution. A comparative performance analysis illustrates their diverse applications in wireless communication, radar systems, satellite communication, and sensing. The review concludes with insights into future challenges and opportunities, underscoring the potential of metantennas to enable ultra-thin, conformal, and multifunctional antennas for next-generation systems, and serving as a valuable reference for researchers advancing metantenna technology toward superior performance in compact designs.

INDEX TERMS Electromagnetic metamaterials, leaky wave antennas, meta-atoms, metasurface antennas, subwavelength structures, 5G and 6G communication.

I. INTRODUCTION

Metamaterials are composed of meta-atoms, which serve as their unit cells, and can be approximately regarded as homogeneous Electromagnetic (EM) materials using the effective medium theory [1], [2]. In contrast, Metasurfaces (MTSs) represent a 2-D expansion of this concept and are comprised of planar arrays of uniform or nonuniform meta-atoms. The design of MTSs allows for the attainment of unique characteristics in terms of how space waves are reflected or transmitted and the alteration of the dispersion properties of surface or guided waves [3], [4], [5], [6]. In the field of microwave antenna applications, MTSs are commonly created using a structured pattern of diminutive elements on a grounded surface, either with or without shorting connections (vias) [7], [8], [9], [10], [11], [12]. Conversely, in submillimeter wavelength applications, MTSs can be composed of a densely packed array of metallic pins on a ground plane [13]. Metasurface Antennas (Metantennas) represent the seamless integration of MTSs with traditional antenna technology, where meta-atoms, the fundamental building blocks of MTSs, enable unprecedented control over electromagnetic waves. This integration offers reduced thickness, lower fabrication complexity, and enhanced performance compared to bulk metamaterials [14]. By using MTSs as the radiating aperture, metantennas achieve superior performance in terms of gain, bandwidth, efficiency, and radar cross-section (RCS) reduction, making them highly suitable

The associate editor coordinating the review of this manuscript and approving it for publication was Giovanni Angiulli.

for next-generation communication systems such as 5G and beyond.

Unlike conventional antennas that rely on bulky reflectors or complex feed networks, metantennas utilize sub-wavelength meta-atoms to precisely modulate phase and amplitude, enabling functionalities such as beam steering, focusing, and polarization conversion. This fusion of metasurfaces and antennas into a unified structure [15] has opened up new possibilities for compact, lightweight, and high-performance antennas across diverse applications, including wireless communication, radar, satellite systems, and sensing [16], [17], [18].

The way a metantenna works is rooted in the interaction of electromagnetic waves with the meta-atoms that constitute the MTS. When a Surface Wave (SW) interacts with locally modulated and periodically varying Boundary Conditions (BCs) created by MTSs, it facilitates the replication of a desired aperture field, which then radiates through the Leaky Wave (LW) effect [16], [19]. This mechanism forms the basis for metantenna operation, allowing for precise wavefront manipulation, beamforming, and polarization control. Metantennas are characterized by their low profile, lightweight design, and ease of fabrication, often using standard Printed Circuit Board (PCB) techniques. The integration of the feeding element within the metasurface plane eliminates the need for bulky external reflectors or complex feed networks, further enhancing their practical advantages. These features, along with their ability to finely tailor aperture fields, have led to the development of a variety of innovative metantenna designs in recent research.

The fundamental design of a meta-atom is governed by the concept of sub-wavelength structures. Traditionally, atoms are considered the smallest building blocks of matter. Despite their small size, atoms are so minuscule that even today, humans have limited control over them and cannot alter their internal structures. However, in the context of electromagnetic metamaterials, the definition of ''small'' is relative to the operating wavelength (λ) [17]. A general design rule for meta-atoms in metamaterials and metasurfaces is that their dimensions should be much smaller than the operating wavelength, typically satisfying the $\lambda/10$ criterion [20]. When a structure is reduced to this sub-wavelength scale, it can exhibit effective medium properties, allowing it to manipulate electromagnetic waves in ways that conventional materials cannot.

The electromagnetic properties of metantenna unit cells are defined by their permittivity (ε) and permeability (μ), leading to classifications such as Double-Negative (DNG) and Single-Negative (SNG) meta-atoms. DNG meta-atoms exhibit both negative permittivity (ε) and negative permeability (μ), enabling a negative refractive index, which results in unique wave propagation effects such as super-resolution imaging and improved impedance matching. These materials enhance beam focusing and directivity, which is crucial for high-gain antennas [17], [21]. SNG meta-atoms include either negative permittivity (Epsilon Negative, ENG) or negative permeability (Mu-Negative, MNG), providing selective wave suppression and impedance matching properties. These materials contribute to low-profile, high-efficiency antenna designs, making them ideal for conformal and miniaturized applications. Meta-atoms designed to achieve these properties enable significant enhancements in beam steering, polarization control, and radiation efficiency, making them essential for advanced metantenna implementations [17], [21].

The design of unit cells in a metantenna follows a structured process to achieve the desired electromagnetic response. The dipole mode is often the primary resonant mode of a scatterer, making it the preferred choice for meta-atoms. The first mode in a scatterer's spectrum, the dipole mode, exhibits the smallest electrical size, making it suitable for unit cell designs [22]. A metallic dipole antenna typically has a length of $\lambda/2$, making it too large for sub-wavelength applications. By using Split-Ring Resonators (SRRs) and other compact resonators, the dipole's effective size can be reduced to sub-wavelength dimensions. Increasing capacitance and inductance (e.g., by extending the length or narrowing the gap of parallel strips) enables further miniaturization while preserving resonance properties [3], [17].

Meta-atom geometries such as cylinders, cubes, and spheres must be carefully engineered to satisfy the $\lambda/10$ criterion. Complex structures like cross-shaped, Jerusalem cross, or complementary resonator designs allow for enhanced polarization manipulation and frequency selectivity [20], [22]. Unlike traditional Frequency-Selective Surfaces (FSS) [23], High-Impedance Surfaces (HIS) [24], and Electromagnetic Bandgap (EBG) structures [25], metantennas derive their properties from their constituent elements rather than overall periodicity. As discussed in [26], [27], and [28], FSS and EBG are historically important periodic structures that differ from metasurfaces in both physical mechanisms and functionality. Metasurfaces, in contrast, act as the two-dimensional counterparts of metamaterials, enabling broader wavefront manipulation beyond filtering or bandgap behavior. The periodicity of meta-atoms influences metasurface performance, with nonuniform designs offering greater flexibility for beam shaping and frequency selectivity. The increasing complexity of metasurface design necessitates the use of computational optimization techniques, including genetic algorithms [29], [30] and machine learning-based models [31], [32]. Fabrication techniques such as 3D printing, liquid crystal tunable materials, and liquid metals are being explored to develop reconfigurable and dynamically tunable meta-atoms [33], [34], [35], leading to the advancement of metantennas.

Metantennas have significantly advanced antenna design and wireless communication by enhancing key performance metrics such as gain, directivity, bandwidth, efficiency, and RCS reduction. They are particularly promising for 5G networks, enabling beamforming, polarization control [36], [37],

and frequency-selective surfaces, while their compact design makes them suitable for sensing applications in biomedical, environmental, and security fields, as well as Internet of Things (IoT) and wearable devices. The development of metantennas relies on a fundamental understanding of meta-atom behavior, unit cell design, and material classification. By leveraging double-negative and single-negative properties, researchers can design antennas with improved radiation control and efficiency. The integration of reconfigurable and nonlinear metasurfaces allows for dynamic electromagnetic property modifications, facilitating beam steering and frequency generation. Additionally, metantennas can be combined with sensors, Radio Frequency Identification (RFID), and other emerging technologies to develop innovative systems. However, challenges remain in scalable fabrication, seamless integration, and application-specific optimization. The ongoing advancements in sub-wavelength unit cell optimization and fabrication techniques continue to drive the evolution of metantennas. Rather than serving as mere enhancements to conventional antennas, metantennas are evolving into independent radiating structures, with advancements in materials and Artificial Intelligence (AI)-driven design expected to shape the future of wireless communication, radar, satellite, and sensing technologies. Fig. 1 illustrates general application scenarios of a metantenna system designed for Fifth Generation (5G) and beyond communication systems, leveraging a mesh-type network topology for flexible and adaptive network deployment. The metantenna enables dynamic beamforming and multi-beam steering, crucial for supporting high-speed, low-latency communication. Additionally, the integration of Reconfigurable Intelligent Surface (RIS) and smart radio environments enhances signal propagation [38], [39], [40] by mitigating multipath effects and improving spectral efficiency. This system is particularly beneficial for Autonomous Aerial Vehicle (AAV)-assisted networks, vehicular communications, and smart city applications, where obstacles can disrupt direct line-of-sight communication. Operating in Millimeter Wave (mmWave) and sub-THz frequencies, such technologies are expected to revolutionize next-generation wireless networks. Furthermore, metantennas play a key role in satellite communication by enabling efficient downlink/uplink connectivity and adaptive coverage for space–terrestrial integrated networks.

This article presents several novel contributions to the field of metantennas, including the first comprehensive classification and detailed analysis of various metantenna types. It provides a comparative performance evaluation, highlighting their advantages, limitations, and applications in wireless communication, radar, and satellite systems. To further strengthen the technical depth, it examines unit cell design mechanisms through equivalent circuit modeling, offering intuitive and design-oriented insights into how different unit cells govern metantenna performance, an aspect not systematically addressed in earlier reviews. It also explores emerging materials and fabrication techniques, such as liquid crystals, liquid metals, and 3D printing, which are shaping

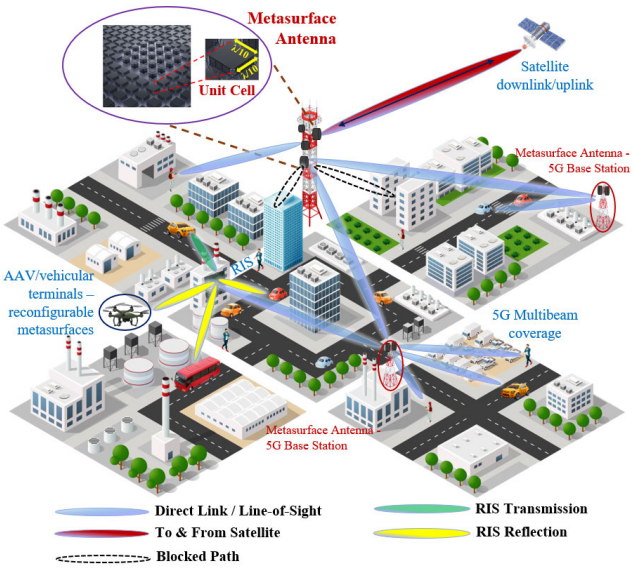

FIGURE 1. General application scenarios of Metasurface Antennas (Metantennas) in next-generation wireless networks.

the evolution of metantennas. Unlike conventional reviews, this work bridges the gap between metasurfaces and antenna technology by emphasizing how metantennas employ

metasurfaces as primary radiating apertures rather than supplementary components, thereby enabling superior performance in gain, bandwidth, efficiency, and radar cross-section reduction. In addition, it identifies key challenges and future research directions, including reconfigurable metasurfaces, miniaturization, and AI-driven optimization, making it a valuable reference for researchers in both academia and industry. By synthesizing classifications, performance analyses, design methodologies, and future prospects, this review provides a comprehensive overview of metantennas and serves as a valuable reference for researchers and professionals, particularly for applications in next-generation communication systems such as 5G and beyond. In that manner, the first section describes the classification of EM MTSs and MTS-based antennas. In the following section, metantennas are illustrated in detail, with several types described along with their respective advantages and challenges. A comparative performance analysis of different categories of metantennas is then presented in categorized tables. In addition, the limitations of current designs, unit cell design mechanisms, and potential future developments and challenges are discussed. The next section describes how metantennas have seen significant advancements through the incorporation of novel materials and fabrication technologies. Finally, concluding remarks are provided in the last section.

II. CLASSIFICATION OF ELECTROMAGNETIC METASURFACES AND METASURFACE-BASED ANTENNAS

A. CATEGORIZATION OF ELECTROMAGNETIC METASURFACES

MTSs can be categorized using several approaches. One common method is based on their operational frequency,

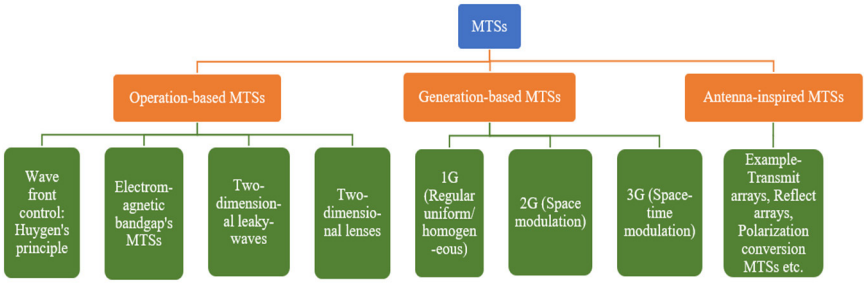

FIGURE 2. The classification of MTSs based on their operation [41] and the generation [42].

distinguishing between MTSs designed for optical or microwave applications. The classification of MTSs can be broadly divided into three categories: operation-based MTSs, generation-based MTSs, and antenna-inspired MTSs, shown in Fig. 2. Each category provides a unique perspective on how MTSs are designed, developed, and applied.

1) OPERATION-BASED MTSS

They are categorized based on their functional mechanisms in manipulating electromagnetic waves. These include wavefront control, guided by Huygens' principle, where the wavefront is shaped to achieve desired behaviors. Electromagnetic bandgap MTSs are designed to block specific frequency bands to regulate wave propagation. Two-dimensional leaky-wave MTSs enable the gradual dispersion of energy in a controlled manner, while two-dimensional lenses act as flat lenses for focusing electromagnetic waves efficiently without requiring bulky curved surfaces [41].

2) GENERATION-BASED MTSS

They focus on the evolutionary stages of metasurface development [42]. First Generation (1G) describes the uniform or homogeneous MTSs with consistent structures, Second Generation (2G) introduces spatial modulation, enabling the MTS to alter its properties across its surface, thereby achieving complex functionalities like beam steering and wavefront manipulation, Third Generation (3G) represents the MTSs that modifies its attributes with space and time both enabling the MTSs dynamic, reconfigurable, and adaptive. This allows for real-time control of electromagnetic waves and expands the scope of their applications.

- *First Generation (1G):*The concepts related to MTSs have been explored since the 1970s and 1980s, primarily in the form of FSSs. FSSs, consisting of periodic arrays of conducting patches or apertures, have been employed for applications such as frequency-dependent mirrors and filters. The understanding of FSSs has evolved from optical diffraction gratings [42].
- *Second Generation (2G):*The transition to the second generation of MTSs spans from 2010 to 2020. During this phase, aperiodic MTSs with spatially varying boundary conditions emerged. There are two categories of nonuniform MTSs: those designed for space-wave control and those for in-plane SW and LW control. Notably, the introduction of the concept of Huygens' MTS is regarded as transparent MTSs that transform wavefronts and enable applications like thin lenses and beam deflectors [42].
- *Third Generation (3G):*The ongoing transition to the third generation of MTSs is where boundary conditions change both in space and time, becoming controllable and intelligent. Reconfigurability is achieved through electronics, time-varying materials, or switchable feed points distributed over the MTSs. Concepts like ''digital-coded MTSs'' and ''programmable MTSs'' are introduced, allowing for the control of various functionalities based on different digital states of the elements. The self-adaptive and cognitive MTSs are also potential candidates [42].

3) ANTENNA-INSPIRED MTSS

These MTSs draw inspiration from traditional antennas. The characteristics of these MTSs first closely match those of conventional reflect-array and transmit-array antennas [43], [44]. This marks the initial encounter between MTSs and antennas. The basic building blocks of traditional transmit-arrays and reflect-arrays consist of antenna radiators that are $\lambda/2$ in size, such as metal patches [45]. These $\lambda/2$-sized radiators can alter the phase profiles of reflected or transmitted waves on two-dimensional planes by integrating phase shifters, lumped elements, delay lines, and related features [44]. This manipulation shapes the wave fronts of the waves based on planar configurations, deviating from the use of parabolic reflectors or convex lenses. On the other hand, functional MTSs utilize sub-wavelength meta-atoms as building blocks, introducing spatial phase variations without the need for extra accessories. Consequently, MTSs provide more customization options for the wave-fronts of transmitted or reflected waves. Motivated by transmit arrays and reflect arrays, diverse MTSs have been created with distinctive characteristics, including anomalous refraction and reflection for beam steering [46], [47], and transmissive or reflective focusing for achieving higher directivity [48], [49]. Furthermore, by employing active phase-shift characteristics, similar to transmit or reflect array antennas, programmable and reprogrammable, reconfigurable MTSs enable dynamic switching

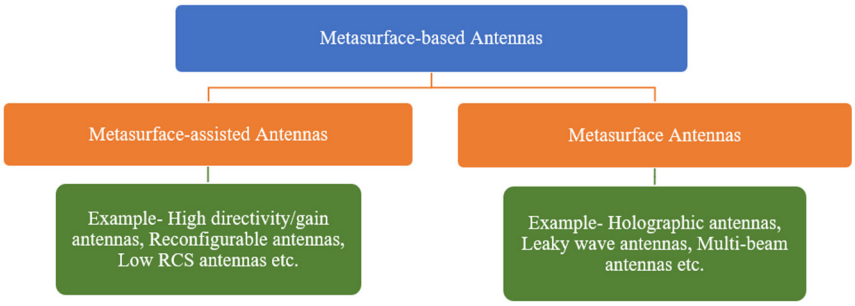

FIGURE 3. The classification of metasurface-based antennas based on the functions of MTSs [17].

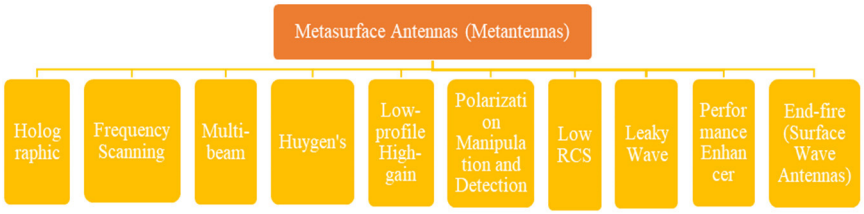

FIGURE 4. A classification scheme for metasurface antennas (metantennas).

functionalities [50], [51]. The theory of phased array antennas elucidates these distinctive modulations of electromagnetic waves.

Last but not least, another classification has been reported for metasurface-based antennas by the functions of MTSs [17]. Metasurface-based antennas have been classified into two broad categories: antennas assisted by MTSs, and metasurface-antennas (metantennas), showcased in Fig. 3.

B. METASURFACE-BASED ANTENNAS

MTSs can be utilized to improve the performance of antennas, including enhancing characteristics like gain [46], [47], [48], [52], bandwidth [53], [54], Axial Ratio (AR) [55], and aperture efficiency [56]. In these setups, the MTS and antenna are typically designed independently and then integrated. The MTS serves as an additional component that enhances the antenna's performance. If the MTS is removed, the antenna can still function, but with reduced performance. As a result, antennas with this type of configuration are referred to as metasurface-assisted antennas.

As MTSs continue to advance, their design methodology is progressively integrated into antenna design. Instead of acting as supplementary superstrates or substrates, MTSs are utilized directly as antennas' radiator-aperture [57], [58], [59], facilitating the seamless fusion of MTSs and antennas. In this merged configuration, the meta-atoms of MTSs function as the radiator elements of array-antennas, while the MTS itself serves as the radiating aperture. This approach, utilizing the MTS as both the radiating aperture and for its other electromagnetic functionalities, has led to the proposal of various innovative MTS antennas. These include end-fire antennas, frequency scanning antennas, lower Radar Cross Section (RCS) antennas, and more. At the present point, the MTS and antenna are combinedly designed like an indivisible element, merging together seamlessly to form a unified entity known as ''metantenna'' [17], leveraging the combined strengths of both components.

III. METASURFACE ANTENNAS (METANTENNAS)

The metantenna is composed of a collection of meta-atoms arranged over a structure that is large electrically. Every meta-atom size is in the sub-wavelength range and is positioned at a distance from its neighboring atoms that is also in the sub-wavelength range [20]. Typically, a metantenna includes an MTS along with one or multiple feeds, where the MTS serves as the aperture of the antenna, while the feed is often positioned at either end or at the center of the MTS. The antenna and MTS are combined together like a unified structure, giving rise to the term ''metantenna'' to describe this fusion [17]. In this setup, the MTS functions like the antenna's aperture, emitting or receiving electromagnetic waves through the feed. Apart from wave radiation and reception, MTSs can also incorporate various additional functionalities depending on the frequency band and polarization, such as multiple beams, holography, frequency scanning, polarization manipulation and detection, lower RCS, enhanced isolation and expanded bandwidth, and many more. This section provides a brief overview of the recent developments in ''metantenna'' technology. Metantennas can be further categorized as embodied in fig. 4.

A. HOLOGRAPHIC METANTENNAS

The optical concept of holography can also be applied to explain the operation of a unique class of leaky-wave

antennas, holographic antennas. In the case of a holographic antenna, the radiating aperture is constructed using a hologram, which receives input from surface-wave modes traveling on thin substrates. This hologram is essentially the result of combining the traveling surface wave with the radiated plane wave, forming an interference pattern. Consequently, it becomes feasible to manipulate the direction and shape of the antenna's beam by altering the hologram's configuration. In comparison to other types of leaky-wave antennas, holographic antennas offer advantages in terms of both manufacturing and system integration, rendering them highly promising for various millimeter-wave applications such as radar systems [60]. The typical holographic antennas have drawbacks in terms of low aperture efficiency and a complicated beamforming feeding network. With the help of the MTS structures, holographic metantennas provide extraordinary performance such as beamforming and frequency scanning with multiple polarizations, high gain, narrow beam width, and lower profile [8], [61], [62], [63], [64], [65].

The mechanism of a scalar impedance holographic MTSs and a comparative study of the operation of Holographic Artificial Impedance Surface (HAIS) at phase crossover and non-phase crossover frequencies have been presented in [8]. The proposed modified-HAIS design is intentionally operated at a non-phase crossover frequency to obtain a null in the azimuth component along the desired direction, and it has improved beam-forming capabilities compared to the conventional HAIS. The article claims a pencil-beam with higher aperture efficiency can be achieved with a modified-HAIS whose physical area is $18.5\lambda^2$. However, the circular polarization criterion has barely been met. Reference [61] presents a low-profile, straightforward holographic metantenna design using a printed circuit board-based Parallel-Plate Waveguide (PPW), capable of generating radiation patterns with dual polarization and multiple beams. The MTS is created using an arrangement of unit cells with slot-like shapes that are subwavelength in size, coupled to a reference wave launched into the PPW utilizing only one coaxial feed. The proposed dual-polarization multibeam metantenna consists of a dielectric substrate with copper-clad surfaces on both sides. The front surface of the antenna is patterned into an array of slot-shaped subwavelength unit cells. The generation of the metasurface-encoded multibeam patterns is achieved using a holographic principle, by interacting the PPW guided-mode reference with the metasurface layer. Although vertical and horizontal polarization have been claimed but supporting evidence was not produced.

The proposed Si/GaAs metantenna design in [62] appears to be a promising solution for high-performance and low-profile antennas at W-Band (75-110 GHz). The study demonstrates that the holographic approach allows for the molding of the radiated beam, resulting in a high directivity of 31.9 dBi and a low-profile design [fig. 5 (a)] appropriate for compact platforms such as CubeSats/SmallSats. The exemplar demonstrated in the study achieved a reflection coefficient

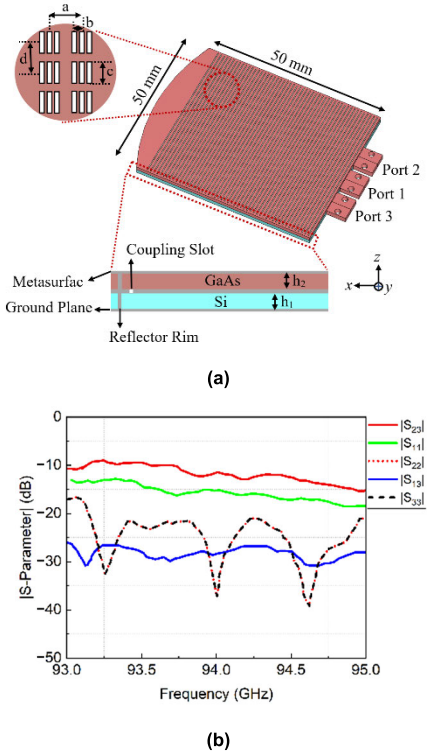

FIGURE 5. (a) Holographic metantenna, pillbox structure loaded with the metasurface layer, (bottom) cross-section of the antenna in the xz plane is shown as an inset. Dimensions: a = 0.85 mm, b = 0.17 mm, c = tapered from 0.38 to 0.4 mm, d = 0.53 mm, h1 = 0.35 mm, h2 = 0.175 mm (b) S-parameter patterns for the Si-GaAs holographic metantenna [62].

below −15 dB at 94 GHz, depicted in Fig. 5 (b), which is a desirable characteristic for efficient signal transmission and reception. However, enough evidence was not provided for the multibeam characteristics, which were claimed in the article. The Kymeta's electronically-scanned antenna technology, which is based on the concept of holographic beam forming implemented through a diffractive metasurface and liquid crystal display technology was presented in [63]. The technology suggests dynamic beam pointing and polarization control, which are essential for meeting the demands of today's communications networks. The challenges involved in developing user terminals for non-geostationary satellite networks, where dynamic beam steering antennas are needed to maintain a link as satellites change position in the sky, were also discussed. They suggest that electronically steerable flat panel antennas may be the only solution to this complex problem. Overall, the article provides valuable insight into the technology behind electronically-scanned antennas and the potential applications for this technology in industries such as transportation, telecommunications, and defense, but the antenna's capability for beam pointing and polarization control was not elaborately discussed.

A novel approach to metantenna design using the one-dimensional holographic concept has been presented in [64]. The proposed metantenna achieves beam-tilt with

fewer unit cells, simplifying the design process and resulting in a more compact structure. The proposed metantenna achieves a continuous beam-scanning angle with high gain. However, it is worth noting that the article focuses on the design and validation of the proposed metantenna using the one-dimensional holographic concept and does not provide a comprehensive comparison with other relevant existing metantenna designs. The modified plane-wave surface wave launcher enhances the frequency band of impedance matching and antenna radiation efficiency, but increases the overall volume of the design by not being conformal.

A new kind of metantenna, the Frequency-Diverse Holographic Metasurface (FDHM) antenna, which produces randomly frequency-diverse radiation patterns, has been demonstrated in [65]. The proposed near-field microwave computational imaging system is built using the FDHM antenna, and it achieves high-quality imaging with a much smaller number of measurements than traditional imaging systems. The compressed sensing technique and iterative shrinkage/thresholding algorithms are applied for the imaging reconstruction. The achieved compressive ratio of this computational imaging system on the physical layer is 30:1. The proposed FDHM antenna and the near-field microwave computational imaging system have potential applications in various fields, such as medical imaging, security screening, and non-destructive testing. However, it is worth noting that the demonstration of the feasibility of achieving computational imaging by the FDHM antenna is conducted by numerical analyses, and experimental validation is yet to be performed. Additionally, the proposed system is based on reflected signals in the frequency domain, which may limit its applicability in certain scenarios.

B. FREQUENCY SCANNING METANTENNAS

A frequency scanning metantenna is an advanced electromagnetic device that operates by dynamically adjusting its electromagnetic properties to steer, focus, and control the direction of incoming or outgoing electromagnetic waves over a range of frequencies. Phase Gradient Metasurface (PGM) is an important early metasurface that enables phase gradients within the plane for waves that are transmitted or reflected [66], [67], [68]. Within the metasurface plane, the phase gradient deflects the antennas' primary lobe direction by acting as a wave vector. The dispersive nature of these phase gradients, caused by resonance phases, leads to frequency scanning as the position of the primary lobe changes with frequency. In-plane feed planar antennas are a common configuration for metantennas, where the metasurface aperture's phase gradient is greater than the wave vector of free-space [69]. Incident waves are converted into Spoof Surface Plasmon Polaritons (SSPPs) through reflective or transmissive PGMs, propagating along the metasurface and concentrating into the feed. During the radiation process, electromagnetic waves on the surface from the feed are transformed into propagating waves in free space, facilitated by

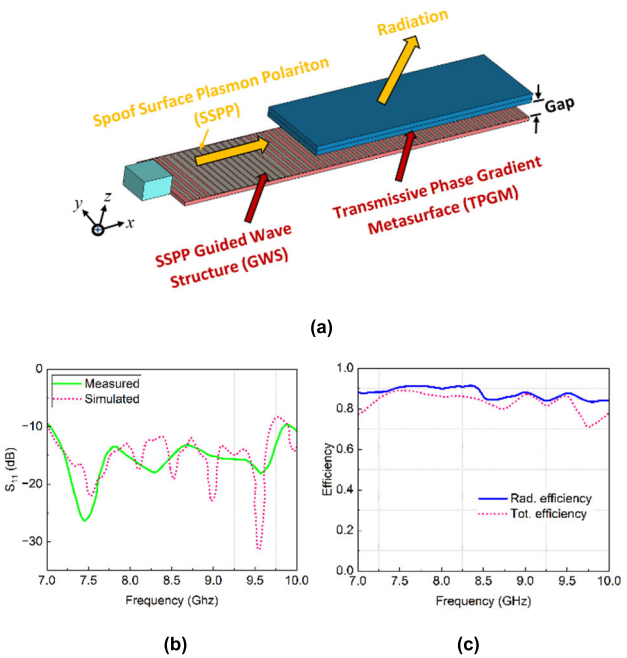

FIGURE 6. (a) Schematic diagram of the Spoof Surface Plasmon Polaritons (SSPPs) planar antenna based on Transmissive Phase Gradient Metasurface (TPGM) (b) Simulated and measured reflection coefficient $|S_{11}|$ (c) Simulated results of the radiation and total efficiency [58].

the antiparallel phase gradients of the MTS [58], [70], [71]. The direction of the main lobe of the antenna changes as the operating frequency varies due to the dispersive nature of the phase gradient provided by the metasurface.

The design and analysis of a novel SSPP planar antenna based on Transmissive Phase Gradient Metasurface (TPGM) has been presented in [58]. The SSPP planar antenna offers advantages over existing planar antennas, including wideband frequency scanning, higher efficiency, and greater design

flexibility. The antenna consists of TPGM placed above the SSPP guided wave structure shown in Fig. 6, exhibiting a directive radiation pattern described by the generalized Snell's law. The SSPP planar antenna can achieve wideband frequency scanning from backward to forward from 7 GHz to 10 GHz, with a maximal total efficiency higher than 90%. Still, it is difficult to further improve the antenna efficiency due to the Driven Surface Wave (DSW) coupling and decoupling by means of reflective PGM, which is not an eigenstate of EM waves and can experience severe scattering before coupling to an eigenmode SSPP, leading to a fast attenuation of field intensities during the transmission process. Reference [50] presents a study on a carefully designed gradient meta-surface that supports high-efficiency anomalous reflections for near-infrared light. The authors demonstrate that the meta-surface can achieve broadband anomalous reflection with high efficiency, and that the reflected wave becomes a bounded surface wave as the incident angle exceeds a critical value. The study also compares the performance of the gradient meta-surface to

previously fabricated gradient meta-surfaces in the infrared regime and discusses potential applications of this technology in shorter wavelength regimes. Additionally, while the study demonstrates high efficiency for anomalous reflection at normal incidence, it is unclear how the performance of the meta-surface would be affected by changes in incident angle or polarization. A method of achieving frequency scanning radiation using decoupling spoof surface plasmon polaritons via phase gradient metasurface has been proposed in [70]. The proposed approach allows for continuous beam scanning and has the potential to be expanded for creating adaptable frequency scanning antennas along curved contours. A prototype antenna operating at 8.8-10.7 GHz was designed, fabricated, and measured, and the results show the high-efficiency beam scanning performance of the prototype. The method can be an effective alternative to the design of either planar or conformal frequency scanning antennas due to its low loss, low profile, low cost, and simple fabrication. Although the side lobes in the radiation pattern are mainly attributed to the nonuniform leakage constant, which is caused by inconsistent resonant amplitudes of the Corrugated Metallic Strip (CMS), this may affect the overall performance of the antenna. Here, an approach to frequency scanning is demonstrated using a planar antenna based on SSPP. The antenna, consisting of a phase-gradient metasurface and a feed structure, operates effectively within a 0.6 GHz bandwidth, maintaining a low reflection coefficient and consistent gain. The antenna can couple the wave from the feed into a spatial radiated wave whose beam pointing angles at 8.9, 9.1, 9.3, and 9.5 GHz are $-12°$, $-8°$, $-4°$, and $0°$, respectively, which verifies the radiation mechanism and frequency scanning feature of the antenna. On the contrary, exciting SSPP through the feed structure is more difficult and inefficient compared to exciting Transverse Electromagnetic waves (TEM) due to the particularity of the field distribution.

C. MULTI-BEAM METANTENNAS

Through the strategic arrangement of meta-atoms with diverse properties on a 2-D plane, it becomes viable to generate phase-gradients focused towards various directions in azimuth. As a result, surface mode electromagnetic radiations could be disengaged from the feed, enabling them to propagate in various directions within free space. This exciting capability unlocks possibilities for designing multi-beam metantennas. Two common arrangements are used to achieve multibeam functionality [72], [73], [74], [75]. In the first approach, the metasurface aperture is divided into angular sectors, each dedicated to generating a beam in a specific direction. Alternatively, the second configuration involves overlaying multiple phase modulations on the metasurface aperture, resulting in higher gain compared to the first configuration. Additionally, by programming the patch antenna arrays' antenna components' feeding phases, it becomes feasible to implement multibeam metantennas directing multiple radiated beams toward different directions using specific coding sequences [76]. Furthermore, multi-beam planar antennas

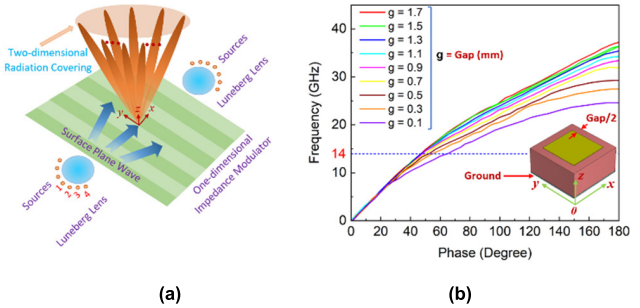

FIGURE 7. (a) Schematic of the entire multi-beam metantenna system, capable of performing two-dimensional beam scanning in free space. The radiation aperture is the 1D impedance-modulator metasurface, and the feeding network is the Luneburg lenses. The unit cells depicted in (b) comprise all metasurfaces. These unit cells can be represented as the surface impedance and the surface refractive index. Because of the x and y axes' symmetry, only ports 1-4 are examined in the experiments' radiation results. (b) Diagram of the fundamental unit cell, where the unit's period was 2.5 mm. Under various gap sizes, the textures' dispersion curves are provided [72].

can be created by directing surface-waves from various feeds upon MTSs because the MTS effectively isolates surface-waves, allowing them to radiate independently [77].

The metasurface system proposed in [72] achieves multi-beam by using two surface Luneburg lenses as the feeding network, illustrated in Fig. 7, which can transform point sources located near the Luneburg lens into surface plane waves propagating in various directions. Next, the One-Dimensional (1D) impedance MTS is positioned between the Luneburg lenses modulates the surface plane waves with

distinct wave vectors. Ultimately, the surface waves radiate into free space after leaving the impedance metasurface. By merely altering the feeding position and operating frequency, the radiation beams can then encompass the 2D spatial scanning region. With the help of the working frequency, the spatial waves can also be scanned in the elevation plane, or roughly the x–z plane. Therefore, unlike a conventional phase-array system, the entire metasurface system may achieve 2D spatial beam scanning by just altering the feeding point and operating frequency. However, because of the leaky wave's attenuation loss, the low-profile system's aperture efficiency was not very great. The design of multi-beam antennas using a single metasurface aperture has been explored in [74]. The authors investigate feeding methods that are single-source and multisource, and they offer closed-form formulae for the metasurface surface impedance in each suggested solution. They also compare the performance of the different designs in terms of beam efficiency, side-lobe level, and cross polarization. Overall, the study shows that metantennas can provide a low-complexity solution for multibeam applications with higher beam efficiency and low cross-polarization. In order to validate the performance of both single-source and multisource feeding schemes, a comparison of the performance of these designs with other existing multibeam antenna solutions needs to be done. In [75], a technique for creating holographic leaky-wave metasurfaces that can execute intricate multi-beam radiations while scanning

frequencies is showcased. The proposed theory allows for one- and two-dimensional multi-beam scanning by varying the frequency. The authors described two methods for recording the appropriate interferograms: one method records the interferograms on the entire metasurface while side feeding, while the other method records the interferograms on a few of the metasurface's subdomains while central feeding. The experimental results agree with numerical simulation and theoretical predictions. The simulation results have confirmed the ability to provide strict frequency-based restrictions on electromagnetic radiation. However, because of the extremely difficult experimental procedure based on their existing measuring apparatus, the measurement has only been possible for three-beam radiations with 2D frequency scanning. A novel surface-wave-based high-impedance surface multi-beam antenna with full azimuth coverage is presented in [77]. With a tilted elevation angle, the suggested antenna design enables effective azimuthal beam scanning. The use of high-impedance surface technology based on surface waves offers advantages in antenna design, including a relatively compact size and improved radiation performance. The proposed antenna design has an advantage in terms of stability and radiation performance. Experimental results of a prototype of the proposed antenna with 28 feeding ports are illustrated. Though the paper focuses on the azimuth scanning capability of the proposed antenna, its scanning performance in elevation needs to be investigated.

D. HUYGENS' METANTENNAS

Huygens' metantennas (HMSs) operate based on the principles of Huygens' principle and metasurfaces. The core component of an HMS is the metasurface itself, which consists of an array of tiny subwavelength-scale structures called meta-atoms. These meta-atoms are strategically arranged across the metasurface to interact with incoming electromagnetic waves effectively. When an electromagnetic wave encounters the metasurface, each meta-atom imparts a specific phase shift and amplitude change to the incident wave. These individual changes combine across the metasurface, determining the overall impact on the wavefront. Huygens' principle is crucial here, as it treats each point on the wavefront as a secondary source of spherical waves. In the context of the metasurface, each meta-atom becomes a secondary source emitting spherical waves. The constructive interference of these spherical waves forms a new wavefront, which can be precisely controlled. HMSs use this capability to steer the direction of wave propagation, shape the wavefront to achieve specific radiation patterns, and even focus or diverge the electromagnetic beam. These antennas are also highly frequency-selective, and their operating frequency band depends on the design of the metasurface. Engineers can tailor HMSs to operate within specific frequency ranges or even across multiple bands. HMSs find applications in a wide range of fields, including wireless communication, radar systems, and imaging devices. In general, HMSs utilize MTSs and Huygens' principle to control electromagnetic waves meticulously, making them versatile tools in modern technology [56], [78], [79], [80], [81], [82], [83], [84].

A solution to the problem of low-profile devices with very directed beams through the design of cavity-excited HMS has been presented in [56]. The proposed design yields near-unity aperture illumination efficiencies from arbitrarily large apertures, offering new capabilities for microwave, terahertz, and optical radiators. The article also highlights the overall design process that is developed and illustrated, which makes it easier to optimize these devices going forward for a range of uses. The great flexibility in selecting the source configuration, along with the effective semi-analytical method, permits investigating other excitation sources, such as those with varying orientations and current distributions, to further customize the aperture fields. The range of applications could be further expanded by using the suggested technology to construct pencil beam radiators that are both compact and efficient across the electromagnetic spectrum. A simple and comprehensive strategy for synthesizing HMS has been demonstrated in [79]. The design of Huygens' metasurfaces is based on the equivalence principle, where properly engineered electric and magnetic surface currents enable arbitrary control of electromagnetic wave transformations. The proposed strategy builds an equivalent model of the HMS antenna and deals with the designs from the perspective of phase optimization, which is simple and straightforward, as shown in Fig. 8. The algorithm suggests passivity and losslessness of the HMS antenna. Although authors claim the proposed strategy is more comprehensive and easier to implement than existing methods, the performance of the proposed strategy was not compared with existing methods in terms of radiation efficiency, bandwidth, and other metrics.

In addition to the fundamental theory, several works have presented efficient methods for extracting the characteristic parameters of metasurfaces and synthesizing their unit cells [85], [86], [87]. These approaches provide practical guidelines for accurately modeling surface susceptibilities and for realizing passive, lossless bianisotropic metasurfaces. Such methods are highly relevant for advancing HMSs, as they facilitate precise unit-cell synthesis and enable more effective design strategies for applications in beam shaping, polarization manipulation, and wavefront engineering. A novel Offset Electric Dipole Pair (OEDP)-based wideband dual-layer Huygens unit cell that achieves wideband transmission has been reported in [81]. The proposed Huygens' unit cell can provide over 300 degrees phase coverage from 28 to 44 GHz with a less than 3 dB transmission loss. The authors then developed a Rotman lens, a parallel-fed slot antenna array, and a Huygens' metasurface to create a wideband and high-gain multibeam array antenna. This design operates throughout a comparatively large bandwidth (28–32 GHz) and claims it can increase the antenna gain further. While the Huygens' unit cell offers a phase coverage of more than 300 degrees within the 28 to 44 GHz range, its phase shift slope varies with different frequencies, potentially

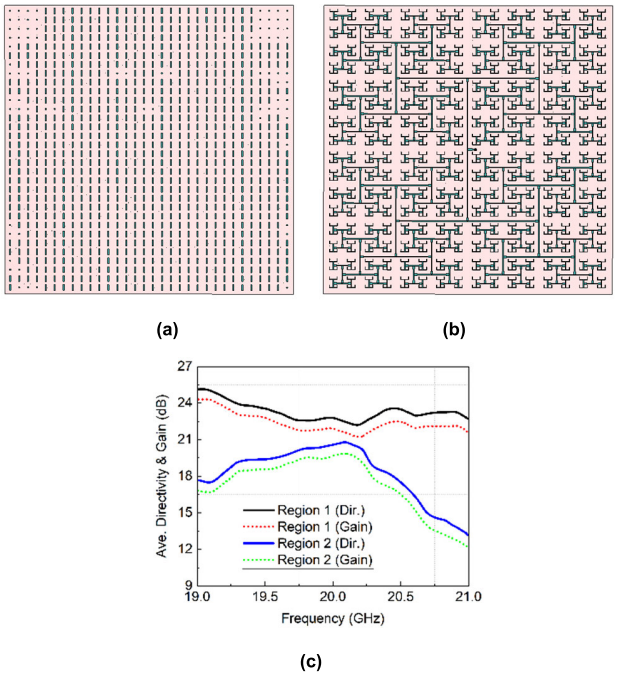

FIGURE 8. (a) Top view and (b) Back view of the HMS (c) Frequency properties of the far fields of the design with smooth phases (average gain and directivity in regions 1 and 2) [79].

introducing additional phase errors when operating away from the central frequency.

A new type of metasurface, called a bipartite Huygens' metasurface, was introduced in [83], which can reflect an incoming electromagnetic wave into any direction with perfect power efficiency. The authors demonstrate that this can be achieved using a passive and lossless metasurface with only two cells per period. Through simulations and experiments, they show that this metasurface can anomalously reflect an incident electromagnetic wave over a wide angular and frequency range. However, the proposed metasurface is limited to reflection angles that are less than 90 degrees, and it may not be suitable for applications that require reflection angles greater than 90 degrees. Reference [84] presents the design and experimental verification of a passive Huygens' metasurface lens for gain enhancement of frequency-scanning slotted-waveguide antennas. The metasurface lens is designed for enhancing the gain of 1-D frequency-scanning slotted-waveguide antennas centered at 34.3 GHz. The paper demonstrates the upward of 13 dB of directivity enhancement achieved by the metasurface lens. The study showcases the versatility of Huygens' metasurfaces in improving the gain and scanning capability of feed antennas. Additionally, the metasurface lens's dispersive focal distance could be modified so as not to have the gain reduction at lower frequencies.

E. LOW-PROFILE HIGH-GAIN METANTENNAS

This type of metantennas are two-dimensional flat array of sub-wavelength scatters with ultrathin thickness, offering unique advantages in antenna design. By serving as antennas' radiation aperture, such metasurfaces enable ultralow-profile antennas with high gain. For high-gain antennas with sub-wavelength interelement spacings, the metasurface unit cell functions as an array element when the constituent sub-wavelength scatters are equal and fed with the same amplitude and phase [57]. The in-plane feed layout is another low-profile high-gain antenna arrangement [71], which allows for narrowband metantennas, involving a single feed situated at the metasurface's extremity. The phase gradient produced by the metasurface is opposite in direction and of identical magnitude to the wave vector of the electromagnetic waves radiated from the feed. Consequently, this setup facilitates the separation of surface mode waves, converting them into propagating waves that propagate freely in free space [59]. Additionally, the use of circular radially modulated anisotropic metasurfaces [88] with a center-fed configuration facilitates double circularly polarized, low-profile, high-gain metantennas that convert cylindrical surface waves into directional radiated waves in the broadside direction. The center-fed-metasurface configurations also enable the implementation of various low-profile antennas, such as low-sidelobe and shared-aperture antennas [89].

The limitations of conventional electrically small antennas and the potential of metasurfaces for developing new antenna applications have been presented in [57]. The metantenna presented in the article is an array of 8×8 electrically reconfigurable resonator elements periodically arranged on a square substrate. The article discusses the metantenna's design, optimization, and performance comparison with a conventional array antenna. The findings indicate that compared to the traditional array antenna, the metantenna has a larger bandwidth and a greater gain. The article concludes that the metantenna concept has the potential to revolutionize the design of antennas and open up new possibilities for antenna applications. While the antenna excels in high gain, it is important to acknowledge its limitations, including the complex design of several layers of the elements and the complex feeding network. Experimental validation of a Ku-band dual-circularly polarized metantenna has been demonstrated in [88] and shown in Fig. 9. The measured maximum gain of the antenna is 23.8 dBi for two different feeding systems. The antenna is an anisotropic single-layer MTS that is radially modulated, which works by exciting two decoupled phase-matched transverse magnetic and transverse electric surface waves with balanced amplitude. These waves interact with the modulated surface, which is an ultrathin grounded dielectric slab printed with subwavelength elliptical slotted metallic patches, leading to a Circularly Polarized (CP) broadside radiation. Two different orthomode transducers have been designed to excite the surface waves with orthogonal polarization and equal amplitude. The first feeding system is composed of a metallic stepped septum inside an air-filled square waveguide, while the second feed is an extremely compact circular waveguide completely filled with

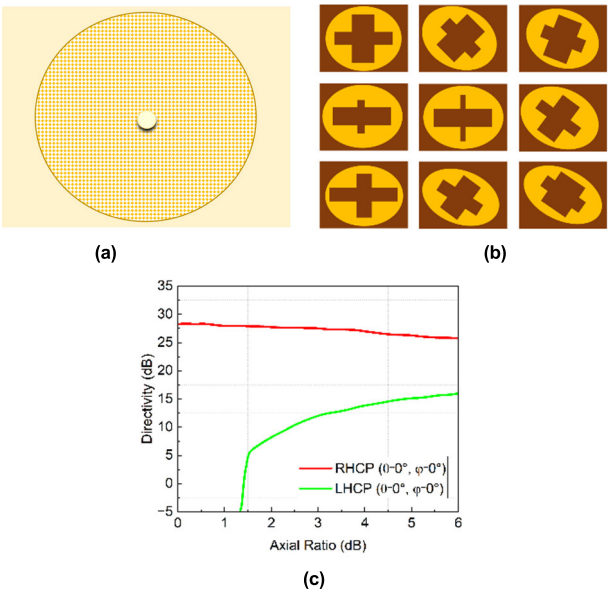

FIGURE 9. (a) Top view (diameter 355 mm) (b) Details of various printed elements of the low-profile high-gain metantenna (c) Effect on the broadside Right Hand Circular Polarization (RHCP) (red) and Left Hand Circular Polarization (LHCP) (green) radiation patterns at 13.4 GHz when the Axial Ratio of the feeding system that excites the metantenna varies [88].

AD1000 dielectric. Yet, the feeding system needs to be more compact to be a low-profile antenna. Reference [89] proposes a metamaterial-like design for a 2D center-fed transmission line grid-antenna with exceptionally high values of aperture efficiency, with a measured gain of 22.22 dB is observed compared to a simulated one of 23.80 dB. The architecture is flexible for different array sizes and scalable to terahertz and millimeter-wave frequencies. The unloaded transmission-line grids can be used as corner-fed Dirac leaky-wave antennas that can produce pencil beams at broadside and tilted angles in the forward and backward radiation directions because they show Dirac cones in the dispersion relation that support both forward and backward wave propagation. When the operating frequency is swept, the pencil beam that is produced sweeps the antenna's E plane. The generated beam nevertheless scans often and does not show a high aperture efficiency, even if it does not divide or deteriorate into a conical beam. Yet, it is not suitable for broadband applications due to the narrow bandwidth of operation.

F. POLARIZATION MANIPULATION AND DETECTION METANTENNAS

Polarization Manipulation and Detection (PMD) metantennas operate based on their ability to control the polarization state, phase, and direction of electromagnetic waves. These antennas consist of carefully engineered meta-atoms arranged in a 2D metasurface. PMD metantennas primarily operate by manipulating the polarization of incident electromagnetic waves. The meta-atoms in the metasurface are designed to interact with incoming waves, altering their electric and magnetic fields to control their polarization. This means they can convert between different polarization states, such as changing linearly polarized waves into circularly polarized ones, or vice versa. These antennas are versatile in their applications. They can not only manipulate polarization but also detect the polarization state of incoming waves. This capability is useful in various fields, including remote sensing and communication, where knowledge of polarization provides valuable information. Moreover, PMD metantennas can adjust the phase of different parts of the wavefront. This feature allows them to steer or shape the radiation pattern of the antenna, which is crucial in applications like radar and satellite communication. One of the significant advantages of PMD metantennas is their compact and lightweight design. Traditional antennas can be bulky, whereas PMD antennas are thin and lightweight, making them suitable for integration into devices and systems where space is limited. As a whole, PMD metantennas are sophisticated devices that leverage engineered meta-atoms to control polarization, phase, and wavefront properties of electromagnetic waves. Their versatility, ability to manipulate polarization, and compact design make them valuable in numerous applications, including communication systems, remote sensing, and imaging [90], [91], [92], [93], [94], [95], [96], [97].

Recent progress on all-dielectric metasurfaces for polarization manipulation has been reviewed in [91]. The article discusses the principles and emerging applications of metasurfaces, which offer a new paradigm for designing ultracompact optical elements with great potential for miniaturizing optical systems. The review highlights the advantages of all-dielectric metasurfaces over plasmonic-type metasurfaces in terms of higher efficiency. The article also discusses the use of anisotropic dielectric nanostructures to support a large refractive index contrast between orthogonal polarizations of light. The emerging applications of metasurfaces in optical systems include polarization detection and imaging, data encryption, display, optical communication, and quantum optics. A novel approach utilizing a phase gradient metasurface for a broadband terahertz polarization converter with anomalous reflection has been discussed in [92]. The proposed polarization converter can manipulate the polarization and wavefront of terahertz waves, and has potential applications in antireflection coating, high-efficiency nondestructive biological sensor, THz detection, imaging, and sensing. According to the simulation results, when the side lobe level is less than -14 dB, the reflecting angle varies from 39° to 22° between 0.40 and 0.60 THz. The increased ratio of polarization conversion achieved by the polarization converter is analyzed through reflection phase and resonant branch analysis. Although it would be beneficial to have experimental results to confirm the effectiveness of the proposed technology. The design and investigation of a novel converter for cross-polarization using an FSS has been presented in [93]. The converter features a rotationally asymmetric fourfold supercell structure that allows for the conversion of an incident wave linearly polarized at any azimuth into the state of cross-polarization, in addition to

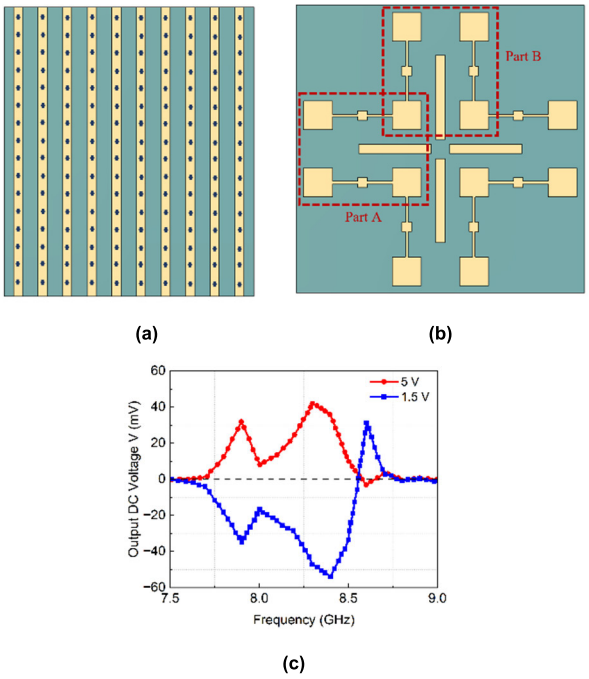

FIGURE 10. (a) Top view of the metantenna, (b) Polarization discrimination antenna, (c) Recorded output DC voltages of the polarization discrimination antenna at various frequencies controlled by the Field Programmable Gate Array (FPGA) while the antennas' distances from transmitting to receiving are one meter [95].

functioning as an FSS filter for circularly polarized waves. The converter has a transmission bandwidth of 3.0 dB and a peak insertion loss of less than 0.16 dB at 5.8 GHz. But the investigation of the cross-polarization converter was limited to a specific frequency band (5.8 GHz). A digital coding metasurface is used in an early version of Polarization Modulation (PoM) for wireless communications, which may dynamically modify the polarization of electromagnetic radiation in a particular frequency range [95]. A schematic of the metantenna is showcased in Fig. 10. With this technology, by regulating the bias voltages on the metasurface in real time, allows binary digital messages to be effectively encoded on the optical rotation states of circularly polarized beams and decoded at the receiving end. The study shows that PoM can enhance physical-layer security in wireless communication systems and provides more flexibility in antenna operating frequencies. Moreover, signal identification requires high power intensity and polarization stability of the receiving EM wave, so there is still an urgency to improve the communication distance through the relay stations. A smart sensing metasurface that can detect microwave incidences in dual-polarization modes and alter the reflected phase configurations using a FPGA as a control mechanism has been showcased in [96]. The metasurface is equipped with incidence detection and 1-bit digital phase modulation, and can achieve self-recognition and determination through a novel sensing mechanism and programmable reaction units. The article presents three schemes containing six coding patterns, two of which are measured and show good agreement with the designs. The authors envision that this work may motivate studies on smart metamaterials with high-level recognition and manipulation. On the other hand, the proposed metasurface was designed to sense and manipulate microwave scattering fields, which limits its further intelligence because of the missing information on the tailoring target.

G. LOW RCS METANTENNAS

Arranging the distributions of the reflection phase in a strategic manner on two-dimensional metasurfaces offers a substantial reduction in monostatic RCS when exposed to plane wave illumination. This reduction is achieved through various mechanisms, including beam splitting, beam deflection, scattering cancellation, polarization conversion, and the widespread absorption of reflected waves [98], [99], [100], [101], [102], [103]. Placing RCS reduction metasurfaces near the antenna element effectively decreases the RCS of planar antenna apertures. The meta-atoms of metasurfaces respond differently to reflected and transmitted waves, enabling a significant reduction in RCS for scattered waves while preserving the antenna's radiation performance for emitted waves. Common configurations for low RCS metantennas involve surrounding the antenna radiator with meta-atoms [104] or arranging antenna components in a configuration akin to RCS-reduction metasurfaces' meta-atoms [105]. Moreover, using antenna elements with diverse configurations on the two-dimensional plane, similar to meta-atoms on RCS-reduction MTSs, can result in high-gain, low RCS planar array antennas. It is also possible to combine meta-atom antenna elements that operate at various frequencies to construct multiband low RCS planar array antennas [106]. In cases where antennas possess substantial metallic regions, like rectangular patch antennas, reflective metasurfaces can be placed atop the metallic patch to achieve RCS reduction through scattering cancellation [107]. For RCS reduction, a 2D Coding Phase Gradient Metasurface (CPGM) is proposed in [99]. The proposed 2D phase gradient modulates the coding element's principal pattern, providing a more adaptable way to manipulate scattering. The particular scattering patterns of the 2D CPGM under phase gradient and coding sequence modulation are analyzed in this research. By adjusting both the phase gradient and the coding sequence, a controlled backward diffusion scattering coding phase gradient metasurface based on Pancharatnam–Berry (PB) phase is produced. Its effectiveness on RCS reduction is demonstrated by both measured and simulated outcomes. Further optimization or improvement of the proposed CPGM design, such as by exploring different coding sequences or phase gradients to achieve better performance or more flexible manipulation of electromagnetic waves, is expected. The reduction of both in-band and out-of-band RCS through anti-phase energy cancellation and scattering has been demonstrated in [101]. The SRRs serve as unit cells of the MTS for RCS reduction and as array elements for linear polarization. The manufactured model working in the X-band has an overall

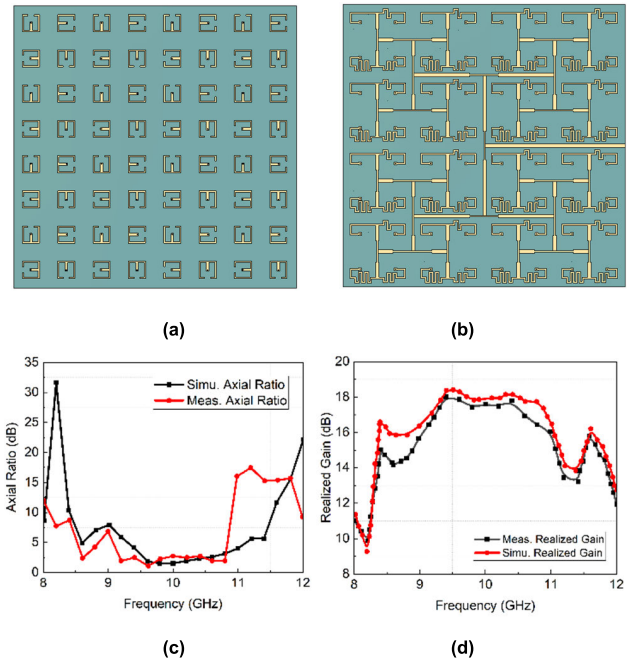

FIGURE 11. (a) Front view, (b) Back view of the metantenna (c) and (d) Frequency response for realized gain and Axial Ratio of the metantenna [101].

bandwidth of 16% with a highest realized gain of 17.9 dB, as shown by the measurements in the paper depicted in Fig. 11. The observed specular reflection has been lowered by 10 dB between 9.2 and 10.8 GHz and by 7.5 dB between 10.8 and 14 GHz under normal lighting conditions. However, the feeding network is a bit complex with respect to the design perspective. A low radar cross-section broadband circularly polarized antenna array using metasurface-based elements have been presented in [104]. The low-RCS characteristic and broadband circularly polarized radiation are both concurrently achieved by the design. The metasurface-based element produces antiphase reflections under orthogonal polarized incident waves, which leads to low RCS. To confirm the design, a 4×4 array prototype was built and measured. The proposed design has potential applications in various fields, such as satellite communication, radar, and wireless communication. Yet, the article does not explore the potential impact of the proposed design on the overall system performance, such as the impact on the receiver sensitivity and the system noise figure. The effectiveness of using randomly rotated components to keep radiation performance high while lowering radar cross section in microstrip phased-array antennas has been demonstrated in [105]. The authors propose a new method for in-band RCS reduction that involves randomly rotating the elements in the array. The results show that this method can achieve significant RCS reduction while maintaining high radiation performance. The article also discusses the use of a cross-shaped metasurface for low RCS. Although the article focuses on in-band RCS reduction, it does not address out-of-band RCS reduction or other aspects of antenna design that may affect RCS. Also, the axial ratio was not described to claim the design as circularly polarized microstrip arrays.

H. LEAKY WAVE METANTENNAS

Leaky-wave metantennas represent an innovative approach to control phase precisely and manipulate electromagnetic waves for various applications in modern technology. These antennas consist of a 2D array of subwavelength-scale elements called meta-atoms. The key principle behind their operation is precise phase control. When an incoming electromagnetic wave, often referred to as a surface wave, interacts with the metasurface, the meta-atoms induce controlled phase shifts in the wave. This interaction causes the surface wave to ''leak'' energy into free space, resulting in radiation away from the surface. By carefully adjusting the phase distribution across the metasurface, the antenna can steer the direction of the emitted beam, a capability known as beamforming. Leaky-wave metantennas operate within specific frequency bands determined by their design. They can also function across multiple frequency bands, enhancing their versatility. These antennas are invaluable for applications requiring accurate and dynamic beam steering, such as in wireless communication and radar systems [108], [109], [110], [111], [112], [113], [114], [115].

The design and experimental results of A miniature magnetic dipole composite Leaky-Wave Antenna (LWA) for right- and left-handed transmission lines with stable wide beam-scanning characteristics have been discussed in [108]. The addition of an alumina ceramic block improves impedance matching and radiation efficiency, resulting in a reliable, broad beam-scanning range and increased antenna gain. The antenna's performance was evaluated through simulations and experiments, and the results demonstrate the suggested design's efficacy. The article also highlights the potential applications of LWAs in various fields, including 5G networks, direction-of-finding, remote sensing systems, near-field-focused antennas, and point-to-point communication. Yet, the presence of the alumina ceramic block imposes constraints on the antenna's applicability, particularly in scenarios where a low-profile design is imperative, like in compact mobile communication devices such as smartphones. [109] discusses the design and implementation of a leaky-wave metantenna for arbitrary aperture synthesis, shown in Fig. 12, which can be used for high-performance low-profile transceivers in wireless communication. The authors introduce the concept of the continuum's quasi-bound states and show how customized perturbations can be used to control the amplitude, phase, and polarization state of metasurface aperture fields. The article also presents several functional capabilities of metantenna prototypes, incorporating far-field beam shaping and single-input multi-output and multi-input multi-output near-field focusing. The authors conclude that leaky-wave metantennas offer a promising solution for meeting the technological needs of 5G/6G networking and broadband satellite internet access. On the other

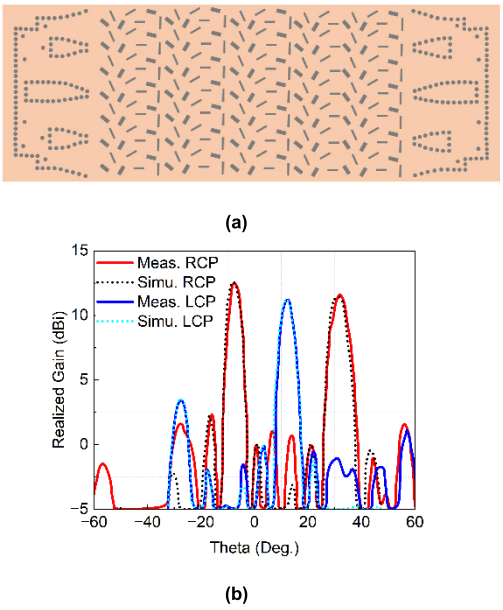

FIGURE 12. (a) Designed Leaky Wave Metantenna (LWM), (b) Realized gain of the LWM (simulated and measured) [109].

hand, the article notes that the multi-beam LWM has a rather low numerically computed radiation efficiency of 44% (including dielectric and conduction loss). This is because the capacity to precisely pattern the amplitude profile of the entire LWM aperture in a point-wise fashion is limited by the tiny perturbation regime, which also limits the degree of asymmetry of each meta-unit. As a result, the antenna designs may not be able to achieve optimal performance in terms of beam shaping and focusing.

In [111], an approach for lessening beam squinting in radiating structures was suggested, with an emphasis on LWAs. The approach uses Huygens metasurfaces to refract the beam without degrading the gain or distorting the beam shape. The metasurface is designed to match the dispersion diagram of the LWA, which dictates its beam-squinting characteristics. According to the experimental results, at angles near broadside, the suggested method can minimize beam squinting by 50% over a 10% bandwidth. However, the need for precise design and fabrication of the Huygens metasurface can be challenging and time-consuming. This article proposes a novel concept of a leaky-wave antenna based on the use of Huygens' metasurfaces. A fishnet-like element has been proposed in [114], allowing a flexible synthesis of the surface impedance, providing very low values of reactance and, thus, very high directivities without requiring an extreme variation of the Periodic Resonant Structure (PRS) geometrical parameters. The remarkably negligible spatial dispersion, together with its negligible modal Transverse Electric-Transverse Magnetic (TE-TM) coupling, allows for a simple but accurate modeling. The proposed Fabry-Perot Cavity LWAs (FPC-LWAs) allow for achieving high radiating performance at a low cost and with low complexity of fabrication. However, a tradeoff is established between Fractional Bandwidth (FBW) and directivity, and lower values of reactance lead to a highly directive FPC-LWA working in a narrow bandwidth, whereas higher values of reactance lead to moderately directive FPC-LWA working in a considerable bandwidth. Using analytical and computational techniques, the radiative performance of several designs for reaching theoretical directivities between 15 and 30 dB is assessed. Although it is necessary to conduct experiments in order to substantiate these findings.

Achievement of controlled radiation by using a bianisotropic metasurface of the omega type in a parallel-plate waveguide is proposed in [115]. The metasurface transforms the guided mode into a leaky mode with arbitrary control of the leakage factor and pointing direction, achieving broadside radiation without degradation. The paper includes simulations and experimental results of two prototypes to validate the proposed concept. The paper concludes that the proposed design paves the way to implement leaky-wave antennas with completely arbitrary radiation patterns. However, several constraints of the proposed design include its unsuitability for wide bandwidth, high gain, and low-profile applications.

I. PERFORMANCE ENHANCER METANTENNAS

Performance Enhancer Metantennas (PEM) have revolutionized the performance of traditional antenna technology. They operate on the principle of using a specially designed metasurface to manipulate incoming electromagnetic waves, resulting in superior antenna performance across various applications. The working principle of these antennas hinges on precise control over the properties of electromagnetic waves, including phase, amplitude, and polarization. This control is achieved through an array of subwavelength meta-atoms embedded in the metasurface. These meta-atoms are meticulously engineered to exert influence over the incident waves, enabling advanced functionalities.

One of the primary advantages of PEM is its capability for beam steering. By carefully adjusting the phase distribution across the metasurface, these antennas can alter the direction in which the electromagnetic waves are emitted. This feature is invaluable in applications such as radar systems, where tracking moving targets requires dynamic beam control. Furthermore, these antennas excel in beam shaping. They can sculpt the emitted beam into various configurations, including narrow, focused beams for long-range communication and wider beams for broader coverage. This adaptability makes them highly versatile and applicable in scenarios where flexible beam patterns are needed. Another critical aspect of these antennas is their efficiency enhancement. Through precise control of wavefronts and phase distributions, they can significantly improve the efficiency and gain of the antenna system. This results in stronger signal transmission and reception, which is essential for reliable communication in various domains. PEM also exhibits frequency selectivity. Some designs are optimized to operate within specific frequency bands, making them suitable for

applications like wireless communication, where efficient spectrum utilization is crucial. Despite their advanced capabilities, these antennas are characterized by their compact and lightweight design. This feature makes them well-suited for integration into devices with space and weight constraints, such as smartphones, drones, and satellite communication terminals. In a nutshell, PEM Antennas leverage advanced metasurface technology to significantly enhance the performance compared to traditional antennas. Their ability to control wavefronts, steer beams, shape radiation patterns, improve efficiency, directivity, gain, and exhibit frequency selectivity makes them invaluable in applications ranging from telecommunications and radar systems to satellite communication. Their compact and lightweight design further underscores their suitability for modern, space-constrained devices [90], [116], [117], [118], [119], [120], [121].

A dual-polarized MRMTA design achieves significant reductions in radar cross section (embodied in Fig. 13) and the ability to steer scattered beams, which are important parameters for many applications [90]. The article discusses the effectiveness of the MRMTA design in achieving quasi-independent radiation and multiple in-band x-polarized scattering manipulations using Characteristic Mode Analysis (CMA). The MRMTA unit cells in radiation and scattering modes have different resonance behaviors around meandering edges and inner slots, respectively. Tuning the inner slots of the MRMTA unit cells can alter the reflection phase distributions for MRMTA's different scattering functions but leave a weak influence on the radiation mode resonance. The antenna's profile is significantly reduced when a metasurface, rather than an accessory, is used as the antenna radiator aperture [116]. This article presents a miniaturized reconfigurable tri-polarization metantenna based on characteristic mode analysis with high-aperture efficiency. The metantenna consists of a single-layered 4×4 array of windmill-like units, wherein PIN diodes can be used to switch between three distinct polarization states for each. The proposed metantenna achieves a high-aperture efficiency of up to 80%. Overall, the use of a metasurface in the design of the metantenna improves its performance in terms of profile, aperture efficiency, and bandwidth. A metasurface structure allows for the optimization of the antenna's radiation performance, resulting in broadband and low-profile RF wireless energy harvesting [118]. By modifying the metasurface structure, the design achieves a harmony between Optical Transmittivity (OT) and electrical performance, resulting in an OT of more than 50%. By integrating radiation and in-band co-polarized scattering functions, an Anisotropic Complementary Metantenna (ACMA) design provides low sidelobe radiation and low in-band co-polarized scattering [119]. ACMA design achieves reduced sidelobe and in-band co-polarized scattering levels below -17.2 dB, ranging from 8.87 to 9.78 GHz. The parameters that have been improved by using a metasurface in [121] are the AR bandwidth and the aperture efficiency of the proposed antenna. The proposed non-uniform metasurface superstrate layer, composed of an array

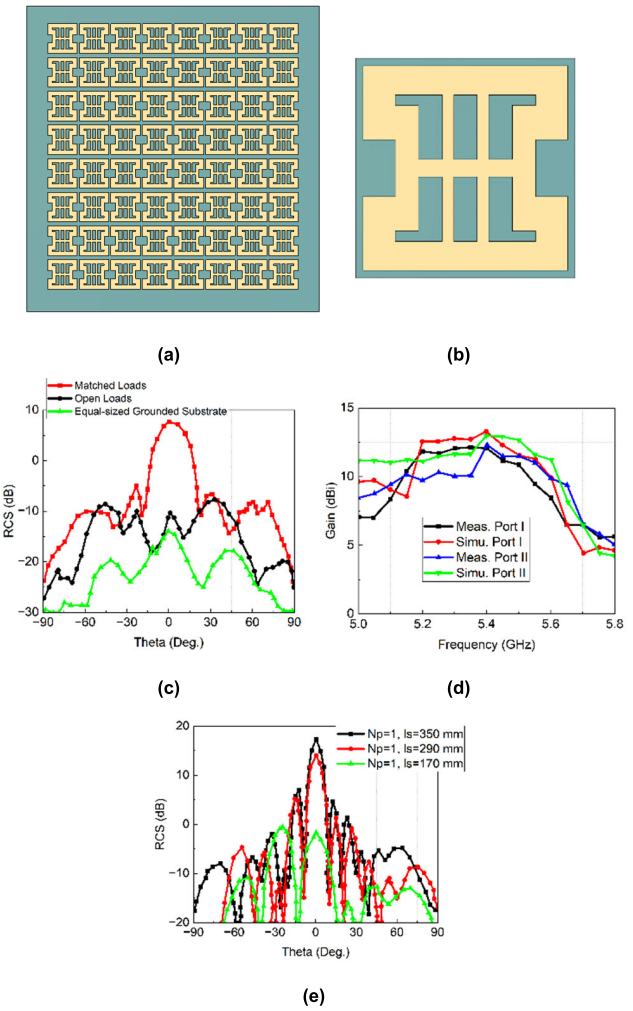

FIGURE 13. Schematic of (a) Multiresonant Metantenna (MRMTA) without feeding structure and (b) its unit cell, (c) Scattering patterns of an equal-sized grounded substrate, open and matched MRMTAs with the random layout at 5.4 GHz in xz plane, (d) Gain fluctuation of MRMTA with the gradient layout, (e) Simulated scattered far fields in xz plane of a gradient MRMTA with fixed MTS and varying sizes of metal ground planes [90].

of 3×4 non-uniform rectangular patches, a finite square ground plane, and a rectangular slot, provides a significant performance enhancement with respect to a uniform metasurface in terms of both AR bandwidth and aperture efficiency. The proposed MTS antenna is compact ($0.068\ \lambda_0$) and provides a remarkable aperture efficiency going from 86 % up to 96 % and an AR coverage in the upper hemisphere greater than 84 % within the desired S-band (2.025 – 2.29 GHz). The use of metasurface in [120] improves the inter-element mutual coupling and reduces the number of phase shifters, which in turn lowers the system complexity and cost.

J. END-FIRE METANTENNAS

End-fire metantennas, also known as end-fire metamaterial antennas, are designed to radiate electromagnetic waves in a specific direction, typically along the axis perpendicular to the antenna's surface, but not necessarily. In order to achieve

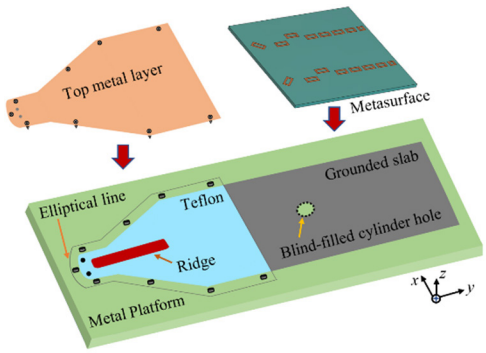

(a)

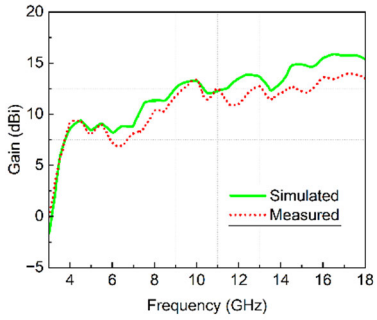

(b)

FIGURE 14. (a) Perspective view of the proposed low-profile End-fire metantenna, (b) Results of measured and simulated gain for the suggested metantenna [122].

high efficiency mutual conversion between radiation waves and surface waves, metasurfaces play a crucial role. Metasurfaces can create surface waves with high coupling efficiency, propagate them along the metasurface with minimal radiation loss, and finally radiate them at the opposite end when placed in the near-field zone of feeding structures such as waveguides or probes. Because of this unique attribute, end-fire antennas can be designed with metasurfaces serving as the main radiation aperture; as a result, they are also known as surface wave antennas. One side of a feeding monopole probe with a metasurface is used in the most basic end-fire design [122]. This article presents a novel design for an end-fire surface-wave antenna with a metasurface coating that achieves a wide bandwidth and low profile demonstrated in Fig. 14. The proposed antenna is compared with previous designs in terms of fractional bandwidth, profile size, gain, polarization, and conformal requirement. The metasurface coating is shown to improve the antenna's performance by suppressing higher-order modes and enhancing the radiation pattern. The air-to-dielectric interface's surface impedance can be altered by the generated electric currents on the metasurface, which can then regulate the transmitted field's phase and magnitude. The scattered fields on either side of the metasurface can be investigated to enhance the antenna's radiation pattern by varying the metasurface's shape and periodicity. The monopole and the meta-atoms' near-field coupling on the metasurface generate and guide surface mode waves to radiate toward the end. Moreover, complex feeding networks, such as those that use patch array metasurfaces as surface wave structures and Substrate-Integrated Waveguide (SIW) power-splitters as substrate-integrated waveguide antennas, can be used to create high-gain end-fire array antennas, enabling the realization of broadband end-fire high-gain antenna arrays [123]. A new high-gain SIW-fed double-layer metantenna array operating at 28–37 GHz is presented in this study. A 1 × 8 SIW power divider is combined with the planned antenna elements, including a double-layer metasurface. The antenna array's simulation gain ranges from 12 to 18.1 dBi between 28 and 37 GHz. The antenna array can be used for end-fire radiation in mm-Wave applications. The Double Layer Metasurface Antenna (DLMA) has better performance than the Single Layer Metasurface Antenna (SLMA) in terms of gain and bandwidth. The bandwidth of the proposed antenna array is 26.1-38.2 GHz and can be simply combined with low transmission loss printed planar antennas. However, precise calculation and design steps need to be followed to design the SIW feed network. Additionally, metasurfaces can incorporate advanced manipulations on surface waves, including focusing, enhancing the versatility and functionality of the metasurface design [124], [125], [126].

A novel implementation of a two-dimensional microwave Luneburg lens antenna with a configurable printed metasurface has been showcased in [124]. By varying the surface impedance inside a parallel-plate structure, the lens is realized by modifying the effective refractive index in accordance with the Luneburg law. An array of circular patches on a planar substrate is used to generate the metasurface, and the patches' sizes are adjusted to change the surface impedance. The article highlights the design criteria and limitations of the metasurface and demonstrates how the lens operation is affected by the metasurface's properties. Based on the conceived lens, A basic parallel-plate antenna that has the ideal height for the waveguide is suggested, and two tapering solutions are proposed to improve the thin parallel-plate waveguide's free space matching. Moreover, the proposed antenna design may not be suitable for broadband applications due to the limited bandwidth of the Luneburg lens.

IV. ANALYSIS AND DISCUSSION

Metantennas have shown great potential in various applications, including 5G and beyond, satellite communications, and phased array antennas. Tables 1 to 10 present a list of various types of metantennas, including their respective sizes, unit cell dimensions, bandwidth and operating frequencies, gain, efficiency, polarization, reconfigurability, validation method, substrate materials, and novelty and applications developed over recent years. The respective brief discussion of these metantennas has been demonstrated in the previous section. These metantennas are designed for different purposes and cover a wide range of applications across various frequency bands, including beamforming, wireless communication, remote sensing, radar, and more. They utilize different substrates and structures tailored to their intended purposes.

TABLE 1. Comparison of Holographic Metantenna design based on various parameters.

Ref.	Overall Size/Unit Cell Dimension	Bandwidth /Operating Frequency	Gain & Efficiency	Polarization, Reconfigurability & Validation Method	Substrate Material	Novelty and Application
[8]	Overall size: 9.55λ × 7.93λ	12 GHz	14.8 dB & 0%-20% aperture efficiency	Dual, not reconfigurable, measurement + simulation	ROGERS 5880, $\varepsilon_r = 2.2, tan\delta = 0.009$	Novel metasurface enables precise beam forming and polarization control; Beam forming
[61]	8.33λ × 8.33λ / 0.21λ × 0.0833λ	25 GHz	10.1 dBi & 38.3%	Dual, reconfigurable, measurement + simulation	Rogers 4003, $\varepsilon_r = 3.38, tan\delta = 0.0027$	Simplified feeding mechanism, no phase-shifting circuits; For selective beam coverage
[62]	Overall size: 15.67λ × 15.67λ	94 GHz	~31.9 dB & ~59% aperture efficiency	Linear, reconfigurable, measurement + simulation	Dual-substrate material, Si ($\varepsilon_r = 11.9$, thickness = $350\mu m$), GaAs ($\varepsilon_r = 12.8$, thickness= $175\mu m$)	Multiple radiation patterns, high directivity (31.9 dBi); Remote sensing instrumentation for NASA's Earth Science missions
[64]	17.92λ × 2.13λ / 0.18λ × 0.18λ at 16 GHz	13-17.5 GHz / 16 GHz	13-15 dBi & 80%-90% radiation efficiency	Dual, reconfigurable, measurement + simulation	Rogers 4003C, $\varepsilon_r = 3.55, tan\delta = 0.0027$	Introduction of a one-dimensional holographic concept; Wireless communication systems (e.g., satellite communication, radar systems, and wireless networks)
[65]	4.84λ × 4.84λ / 0.16λ × 0.16λ at 22 GHz	18-26 GHz	Not mentioned	Not mentioned, not mentioned, theoretical + simulation	Rogers 3006, $\varepsilon_r = 6.15, tan\delta = 0.0025$	Stochastically distributed surface impedance, randomly frequency-diverse radiation patterns; Enhanced near-field microwave computational imaging

The analysis indicates a growing interest in metantennas and their potential for various applications. Each article addresses different aspects of metantenna design, including modeling, beamforming, beam steering, and reconfigurability. The transition to the third generation of metantennas suggests a promising future for metantennas in wireless communication, imaging, and other fields. It's clear that staying informed about developments and innovations in this area is crucial for researchers and engineers to remain at the forefront of antenna design and applications. Here are some limitations of present designs and potential future developments and challenges interpreted from Tables 1 to 10 for metantennas:

A. LIMITATIONS OF PRESENT DESIGNS

- *Limited Bandwidth:* Some metantenna designs, such as Luneburg lens-based metantennas, may not be suitable for broadband applications due to their inherently limited bandwidth.
- *Efficiency and Losses:* Metantennas, especially those based on leaky-wave or holographic principles, can suffer from efficiency losses due to surface wave attenuation, scattering, and other factors. These losses can impact the overall performance, particularly in high-gain or long-range applications.
- *Reconfigurability and Dynamic Control:* While reconfigurable metasurfaces offer dynamic control over electromagnetic properties, achieving real-time reconfigurability with high precision remains a challenge. Current designs often require complex control mechanisms and may suffer from limited response times.
- *Complex Design and Fabrication:* The increasing complexity of metasurface designs necessitates the use of computational optimization techniques, such as genetic algorithms and machine learning, making their practical realization challenging.
- *Scalability Issues:* The development of efficient and scalable fabrication techniques remains a significant challenge, limiting the large-scale implementation of metantennas in commercial applications.
- *Integration Challenges:* Metantennas require seamless integration with other components and systems, such as sensors and RFIDs, to fully realize their potential in advanced communication networks.
- *Performance Trade-offs:* There is often a trade-off between fractional bandwidth and directivity, meaning that optimizing one parameter can negatively impact the other.
- *Material Limitations:* The use of novel materials such as liquid crystals and liquid metals can enhance performance but also introduce reliability concerns due to environmental sensitivity and fabrication difficulties.

B. UNIT CELL DESIGN MECHANISMS AND EQUIVALENT CIRCUIT MODELS FOR METANTENNAS

The performance of metantennas is fundamentally determined by the electromagnetic response of their unit cells. A clear understanding of these responses, together with equivalent circuit models (ECMs), provides intuitive and design-oriented insights into the analysis and design of metasurfaces. Below, we summarize the main classes of unit cells, their working principles, and their corresponding ECMs.

TABLE 2. Comparison of frequency scanning Metantenna design based on various parameters.

Ref.	Overall Size/Unit Cell Dimension	Bandwidth /Operating Frequency	Gain (dBi) & Efficiency	Polarization, Reconfigurability & Validation Method	Substrate Material	Novelty and Application
[58]	Overall size: 9.2λ × 2λ at 10 GHz	7-10 GHz	16.3 dB & 83% radiation efficiency	Linear, not mentioned, measurement + simulation	Dielectric, $\varepsilon_r = 6.15, tan\delta = 0.0009$	Independent design of TPGM and SSPP, Effective polarization conversion; Improving antenna performances
[66]	8.8λ × 8.8λ / 0.088λ × 0.15λ	8 GHz	Not mentioned & up to 99.9%	Linear, not reconfigurable, measurement + simulation	FR4, $\varepsilon_r = 4.3, tan\delta = 0.025$	Impressive coupling efficiency of up to 99.9%, efficient coupling of incident waves into Surface Plasmon Polaritons; Microwave devices, ultra-thin absorbers, high-sensitivity sensors
[67]	-	15 GHz	Not mentioned	Linear, not reconfigurable, measurement + simulation	Dielectric, $\varepsilon = 3.9$	Nearly 100% conversion efficiency without conventional prisms or gratings; High-efficiency surface plasmon couplers, anti-reflection surfaces, light absorbers
[68]	Overall size: 705.88λ × 705.88λ	$\lambda = 850$nm	Not mentioned & up to 80%	Linear, not reconfigurable, measurement + simulation	MgF2, $\varepsilon = 1.892$	First demonstration at 850 nm; Antireflection coatings, optical absorbers, polarization, spectral beam splitters, and high efficiency surface plasmon couplers
[69]	Overall size: 16λ × 16λ	10 GHz	Not mentioned	Linear, reconfigurable, simulation only	Dielectric, $\varepsilon_r = 6.25$	Polarizable particle-based design, dynamic beam forming capabilities; Satellite communications, wireless power transfer, radar imaging
[70]	8.91λ × 0.594λ / 0.165λ × 0.099λ at 9 GHz	8.8-10.7 GHz / 9 GHz	14.2 dB & above 80% radiation efficiency	Linear, reconfigurable, measurement + simulation	F4B, $\varepsilon_r = 2.65, tan\delta = 0.001$	Continuous beam steering and conformal designs; Plasmonic waveguide communication, efficient energy collector, transformer
[71]	5.394λ × 0.72λ / 0.129λ × 0.06λ at 9 GHz	8.9-9.5 GHz	~10 dB & 24%	Linear, not reconfigurable, measurement + simulation	MTS: TACONIC-CER10, $\varepsilon_r = 10, tan\delta = 0.0035$; Feed: FR4, $\varepsilon_r = 4.3, tan\delta = 0.02$	Efficiently manipulates beam direction based on frequency changes; Larger angle scanning antenna

- *Resonant Propagation-Phase Unit Cells:* Patch, slot, ring, and cross-shaped inclusions are commonly used for reflectarrays and frequency-selective surfaces. Their behavior can be modeled using LC resonators, where the capacitance arises from gaps between metallic elements and the inductance from the current path. By tuning these parameters, such cells can provide full 360° phase control at resonance [44], [127]. While compact and effective, they often exhibit a narrow bandwidth due to their high Q-factor nature.
- *High-Impedance and Artificial Magnetic Conductor (AMC) Surfaces:* Mushroom-type structures, consisting of patches connected to a ground plane via vias, act as parallel LC resonators. The capacitance is set by the patch gap, and the inductance by the via and substrate thickness. At resonance, the surface impedance tends toward infinity, creating an in-phase reflection characteristic of an artificial magnetic conductor [128]. These unit cells suppress surface wave propagation and enable low-profile antennas, though their bandwidth remains limited.
- *Huygens' Unit Cells:*Huygens' metasurfaces are realized by balancing electric and magnetic dipole responses. In circuit terms, they can be modeled as matched impedance sheets, with electric dipoles represented as capacitive/inductive elements and magnetic dipoles as loops or apertures. When properly balanced, these cells enable near-unity transmission amplitude with arbitrary phase control, thereby achieving highly efficient transmitarrays and gradient metasurfaces [85], [129].
- *Geometric Phase (Pancharatnam-Berry) Unit Cells:* PB-phase cells impart phase through element rotation rather than resonance, where the imparted phase is given by $\phi = \pm 2\psi$, with ψ as the rotation angle. Unlike propagation-phase cells, their mechanism is explained via polarization transformations and Jones matrices rather than LC circuits. These cells are particularly powerful for circular polarization and orbital

TABLE 3. Comparison of multi-beam Metantenna design based on various parameters.

Ref.	Overall Size/Unit Cell Dimension	Bandwidth /Operating Frequency	Gain (dBi) & Efficiency	Polarization Reconfigurability & Validation Method	Substrate Material	Novelty and Application
[72]	18.67λ × 18.67λ / 0.117λ × 0.117λ at 14 GHz	17-21 GHz	20 dB & not mentioned	Not mentioned, not reconfigurable, measurement + simulation	F4B, $\varepsilon_r = 3.5$, thickness= $1.6mm$	Dual-physics control for 2D spatial beam scanning without active components; Remote sensing, modern wireless communication systems, and radar
[73]	Overall size: 4λ × 4λ, radius of circular aperture = 2λ at 10 GHz	9.5-11 GHz / 10 GHz	Not mentioned	Circular, not reconfigurable, measurement + simulation	Rogers 3010, $\varepsilon_r = 10.2, tan\delta = 0.003$	Independently manipulates two beams with different polarizations; Radar detections, wireless and satellite communications, and imaging systems
[74]	Radius of circular aperture = 12λ / 0.17λ × 0.17λ at 26.25 GHz	26.25 GHz	23.6-28.3 dBi & ~55% aperture efficiency	Circular, reconfigurable, simulation only	Dielectric, $\varepsilon_r = 9.8$, thickness= $0.508mm$	Innovative single-source and multisource feeding schemes, utilization of anisotropic impedance for improved aperture efficiency; Doppler radio-guides and radio altimeters
[75]	13.6λ × 13.6λ / 0.17λ × 0.17λ at 17 GHz	16-18 GHz / 17 GHz	Not mentioned	Dual, reconfigurable, measurement + simulation	FR4, $\varepsilon_r = 4.3, tan\delta = 0.025$	2D beam scanning, holography-leaky wave integration; Satellite communications and radar systems
[76]	Sample 1: 3.73λ × 3.2λ Sample 2: 3.73λ × 4.21λ Sample 3: 4.32λ × 2.96λ Sample 4: 4.14λ × 3.98λ Sample 5: 4.14λ × 3.98λ	3.5 GHz	14.3-15.7 dB & not mentioned	Not mentioned, reconfigurable, measurement + simulation	F4B, $\varepsilon_r = 2.65, tan\delta = 0.001$, thickness= 0.0117λ	Low-profile coding metantennas; Multitasked and intelligent antenna devices
[77]	25λ × 25λ / 0.33λ × 0.33λ at 25 GHz	23-27 GHz / 25 GHz	~3dBi & ~76%	Linear, not reconfigurable, measurement + simulation	Laminate, $\varepsilon_r = 10.2, tan\delta = 0.0035$	Integrated offset reflectors, 360° scanning capability; Surveillance radar applications

angular momentum (OAM) beam generation, though their efficiency is polarization-dependent and bandwidth is limited by polarization conversion [130], [131].

- *Bianisotropic and Omega-Type Unit Cells:* These cells incorporate magnetoelectric coupling, where electric fields induce magnetic moments and vice versa. Their ECMs are expressed in generalized impedance/admittance matrices with off-diagonal terms to represent this coupling. Such designs provide additional degrees of freedom, enabling asymmetric transmission, angularly stable reflection, and perfect anomalous refraction [132].
- *Absorbing Unit Cells:* Metasurface absorbers, such as metal–insulator–metal (MIM) configurations or Salisbury screens, can be modeled using RLC circuits. Here, resistive loading provides loss, capacitance is defined by metallic patches, and inductance arises from substrate thickness. By matching the surface impedance to free-space impedance ($\eta_0 = 377\,\Omega$), such cells achieve perfect absorption, making them valuable for radar cross-section (RCS) reduction and electromagnetic interference mitigation [133].

Recent studies have shown how equivalent circuit models guide practical unit cell optimization. A Leaky-wave Antenna

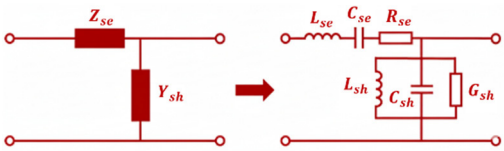

FIGURE 15. ECM of CRLH-TL LWA unit cell [108].

(LWA) unit cells have been modeled in [108] as Composite Right/Left-Handed (CRLH) transmission lines (TL), where the gap and stub acted as series capacitance and shunt inductance, shown in Fig. 15. By enhancing capacitance with an Alumina Ceramic Block (ACB) and varying unit cell dimensions, they achieved miniaturization, stable wide-angle scanning (−70° to +69°), and higher gain (7.7 dBi). This demonstrates how ECM-based analysis links geometry to performance improvements in efficiency, scanning stability, and compactness.

Through equivalent circuit modeling, designers can capture the essential physics of diverse unit cells without resorting immediately to full-wave simulations. Resonant cells provide phase agility but limited bandwidth; AMC structures enable low-profile integration; Huygens' cells achieve efficient transmission; PB-phase cells offer geometric simplicity; bianisotropic unit cells add powerful control; and

TABLE 4. Comparison of Huygens' Metantenna design based on various parameters.

Ref.	Overall Size/Unit Cell Dimension	Bandwidth /Operating Frequency	Gain (dBi) & Efficiency	Polarization Reconfigurability & Validation Method	Substrate Material	Novelty and Application
[56]	14λ × 1.89λ / 0.1λ × 0.1λ	20 GHz	~17 dBi & 81%	Not mentioned, not reconfigurable, measurement + simulation	Rogers RT/duroid 6010LM, $\varepsilon_r = 10.81, tan\delta = 0.0023$; Rogers 2929 bondply, $\varepsilon_r = 2.94, tan\delta = 0.003$	Decoupled excitation and radiation, Near-unity efficiency; Pencil beam radiators
[79]	16.7λ × 16.7λ / 0.25λ × 0.25λ	20 GHz	21.7-23.8 dB & -0.9 dB total efficiency	Linear, not reconfigurable, measurement + simulation	Rogers RO4350B, $\varepsilon_r = 3.66, tan\delta = 0.004$; Rogers RO4450B, $\varepsilon_r = 3.54, tan\delta = 0.004$	Simple phase optimization strategy, enhancing efficiency and practicality; Microwave relay links
[81]	$17.5\lambda_0 \times 18\lambda_0$ / $0.25\lambda_0 \times 0.5\lambda_0$	28-32 GHz / 30 GHz	24.4 dBi & ~7% aperture efficiency	Linear, not mentioned, measurement + simulation	Arlon Cu clad 250GX, $\varepsilon_r = 2.5, tan\delta = 0.0017$, thickness= 0.16λ at 40 GHz	Uses only electric polarizabilities, allowing for wideband transmission and a significant phase shift range; High-gain multibeam array antennas
[82]	$14.99\lambda_0 \times 14.99\lambda_0$ / $0.45\lambda_0 \times 0.45\lambda_0$	24.1-28.2 GHz / 26.2 GHz	30.7 dBi & ~42.25% aperture efficiency	Linear, not mentioned, measurement + simulation	F4B, $\varepsilon_r = 2.2, tan\delta = 0.001$, thickness= $0.131\lambda_0$	Complete phase coverage, simplified vialess design; 5G Millimeter-wave systems
[83]	Unit cell: 0.12λ× 0.12λ	24 GHz	Not mentioned & over 90%	Linear, not mentioned, measurement + simulation	ROGERS 5880, $\varepsilon_r = 2.2, tan\delta = 0.009$	Simple structure using only two elements per period, wideband operation (25.7%) without resonant elements; Practical anomalous reflection metasurfaces
[84]	40λ× 15λ / $0.114\lambda_0 \times 0.114\lambda_0$	33.5-35.3 GHz / 34.3 GHz	~10 dB & 76% transmission efficiency	Linear, not reconfigurable, measurement + simulation	Rogers RO3010, $\varepsilon_r = 10.2, tan\delta = 0.003$; Rogers 2929 bondply, $\varepsilon_r = 2.94, tan\delta = 0.003$	Lightweight design boosts antenna gain by 10 dB; Gain augmentation of slotted waveguide antennas with frequency scanning

absorbers enable stealth and EMC functionality. Together, these approaches form the design toolkit that underpins metantenna development.

Table 11 summarizes the working principles, equivalent circuit models, and performance impact of commonly used metasurface unit cells. Equivalent circuit modeling provides an intuitive understanding and simplifies the design of metantennas by linking geometric parameters to electromagnetic response.

C. POTENTIAL FUTURE DEVELOPMENTS, CHALLENGES, AND SCOPE FOR IMPROVEMENT

- *Advancements in Antenna Design:* Metantennas have the potential to revolutionize antenna design by enabling the development of ultra-thin, conformal, and multifunctional metantennas. These metantennas can be seamlessly integrated into a wide range of devices and systems, paving the way for next-generation wireless communication and sensing technologies.
- *Enhancements in 5G and Beyond Communications:* One of the most promising applications of metantennas lies in 5G and future communication networks, where they can significantly enhance wireless performance. By enabling beamforming, polarization control, and frequency-selective surfaces, metantennas can improve signal strength, reduce interference, and support high-speed data transmission.
- *Advanced Sensing Applications:* Metantennas can be leveraged to develop highly sensitive and selective sensors for diverse applications, including biomedical sensing, environmental monitoring, and security systems. Their ability to manipulate electromagnetic waves at a subwavelength scale makes them ideal for precision sensing and detection.
- *Optimization for Superior Performance:* Future research should focus on enhancing metantenna performance metrics such as gain, directivity, bandwidth, and

TABLE 5. Comparison of low-profile high-gain Metantenna design based on various parameters.

Ref.	Overall Size/Unit Cell Dimension	Bandwidth /Operating Frequency	Gain (dBi) & Efficiency	Polarization Reconfigurability & Validation Method	Substrate Material	Novelty and Application
[57]	1.2λ× 1.2λ / 0.015λ× 0.03λ	3 GHz	~14.7 dBi & not mentioned	Not mentioned, not mentioned, simulation only	Rogers TMM10i, $\varepsilon_r = 9.9, tan\delta = 0.002$; Rogers RT5880LZ, $\varepsilon_r = 1.96, tan\delta = 0.002$	Enhances gain using small resonators and optimized current distribution; Maximum gain in any practically any direction in the half plane
[59]	1.98λ× 0.992λ / Super cell: 0.165λ× 0.165λ	3-3.2 GHz / 3.1 GHz	~9 dB & radiation efficiency ~80% radiation efficiency	Linear, not mentioned, measurement + simulation	FR4, $\varepsilon_r = 4.3, tan\delta = 0.025$, thickness= $0.0517\lambda_0$	Efficient wave coupling, high gain, and compact design; Mobile communication, satellite communication
[88]	Radius $8\lambda_0$ / $0.14\lambda_0$× $0.14\lambda_0$	13.5 GHz	23.8 dBi & 18.2% aperture efficiency	Circular, not reconfigurable, measurement + simulation	Arlon AD1000, $\varepsilon_r = 10.2, tan\delta = 0.0023$, thickness= $0.057\lambda_0$	Innovative feeding systems with a compact, dielectric-filled circular waveguide; Satellite communications, radar systems, and wireless networks
[89]	4.725λ× 4.725λ / 0.53λ× 0.53λ	10.5 GHz	22-23 dB & ~100% aperture efficiency	Linear, not reconfigurable, measurement + simulation	Rogers RT/duroid 5870, $\varepsilon_r = 2.33, tan\delta = 0.0012$, thickness= $0.0275\lambda_0$	Achieves extremely high aperture efficiency (over 90%); Satellite communications, point-to-point communications, collision detection, and automotive radars

TABLE 6. Comparison of polarization manipulation & detection Metantenna design based on various parameters.

Ref.	Overall Size/Unit Cell Dimension	Bandwidth /Operating Frequency	Gain (dBi) & Efficiency	Polarization Reconfigurability & Validation Method	Substrate Material	Novelty and Application
[90]	3.06λ× 3.06λ (one of many types) / $0.27\lambda_0$× $0.27\lambda_0$	5.4 GHz	12.2-12.8 dBi & not mentioned	Linear, not mentioned, measurement + simulation	Dielectric, $\varepsilon_r = 2.2, tan\delta = 0.0009$	Enables independent control of radiation and scattering; achieves finer scattered field shaping
[92]	10λ × 10λ / 0.33λ× 0.33λ at 0.50 THz	0.4-0.6 THz / 0.50 THz	Not mentioned	Converts linear to circular polarization, not mentioned, simulation only	Polyamide, $\varepsilon_r = 3.5$, thickness= $0.0275\lambda_0$	Manipulates both polarization and wavefront simultaneously; Terahertz detection, imaging, and sensing, antireflection coating, high efficiency non-destructive biological sensor
[93]	6.96λ × 6.96λ / 0.35λ× 0.25λ	5.8 GHz	Not mentioned	Linear, not mentioned, measurement + simulation	F4B, $\varepsilon_r = 2.65, tan\delta = 0.002$, thickness= $0.0387\lambda_0$	Low insertion loss and high efficiency; Radomes and wireless communication systems
[94]	Aperture size = $\pi \times 3.67^2\lambda^2$ / 0.49λ× 0.49λ	25-29.3 GHz / 27.7 GHz	23.6 dBi & 43.1% aperture efficiency	Circular, not reconfigurable, measurement + simulation	ROGERS 5880, $\varepsilon_r = 2.2, tan\delta = 0.009$; ROGERS RO4450F, $\varepsilon_r = 3.5, tan\delta = 0.004$	Dual-function metasurface for LHCP transmission and RHCP reflection; Satellite communication, radar 610 detection, and wireless communication systems
[95]	5.64λ × 4.86λ / 0.162λ× 0.27λ at 8.1 GHz	7.9-8.3 GHz	~12 dB & not mentioned	Circular, reconfigurable, measurement + simulation	F4BM, $\varepsilon_r = 2.2, tan\delta = 0.001$, thickness= $0.0387\lambda_0$	Dynamic polarization control, decoupled design, multibit encoding, enhanced security; Multichannel communications
[96]	-	4.95 GHz	Not mentioned	Linear, reconfigurable, measurement + simulation	FR4, $\varepsilon_r = 4.4, tan\delta = 0.025$, thickness= $0.0248\lambda_0$	Integrates real-time sensing and programmable manipulation of electromagnetic fields for dual-polarization modes, enabling simultaneous sensing and response to microwave incidents; Reducing RCS, sensing, and communication systems

TABLE 7. Comparison of low RCS Metantenna design based on various parameters.

Ref.	Overall Size/Unit Cell Dimension	Bandwidth /Operating Frequency	Gain (dBi) & Efficiency	Polarization Reconfigurability & Validation Method	Substrate Material	Novelty and Application
[98]	Overall size: 8λ × 8λ at 10 GHz	9-23.9 GHz	Not mentioned	Not mentioned, not mentioned, measurement + simulation	F4B, $\varepsilon_r = 2.65, tan\delta = 0.002$	Combines topological optimization to achieve simultaneous perfect absorption and scattering reduction; Stealth application and military demands
[99]	Unit cell: 0.2λ× 0.2λ at 11.6 GHz	11.6-18.8 GHz	Not mentioned	Not mentioned, not mentioned, simulation only	Dielectric, $\varepsilon_r = 2.65, tan\delta = 0.001$	Enables simultaneous modulation of array and primary patterns; Radar cross-section reduction
[100]	6.48λ × 6.48λ / 0.132λ × 0.132λ	3.6 GHz	Not mentioned	Linear, not mentioned, measurement + simulation	FR4, $\varepsilon_r = 4.3, tan\delta = 0.025$	Enables a wide bandwidth while maintaining a high polarization conversion ratio; Ultrawideband polarization converters
[101]	Overall size: 3.73λ × 3.73λ	10 GHz	17.9 dB & ~36% aperture efficiency	Circular, not mentioned, measurement + simulation	Rogers RT4735LZ, $\varepsilon_r = 2.55, tan\delta = 0.0026$, thickness= $0.0253\lambda_0$	Achieves high gain and low RCS through an innovative integration of SRRs; High-gain, low-RCS applications
[102]	6λ × 6λ / 0.75λ × 0.75λ at 10 GHz	6.5-20 GHz	Not mentioned	Not mentioned, not reconfigurable, measurement + simulation	Foam board, $\varepsilon_r = 1.1$	Introduction of an absorptive coding metasurface that effectively combines absorption and scattering manipulation; Stealth technology
[103]	0.17λ × 0.17λ / 0.04λ × 0.04λ at 1 GHz	1-6 GHz	Not mentioned	Circular, not mentioned, measurement + simulation	FR4, $\varepsilon_r = 4.3, tan\delta = 0.025$	Enhanced absorption efficiency at low frequencies while maintaining a compact design; Electromagnetic protection, RCS reduction
[104]	2.67λ × 2.67λ / 0.67λ × 0.67λ at 5 GHz	5 GHz	5.7-7.5 dBi & over 70%	Circular, not reconfigurable, measurement + simulation	FR4, $\varepsilon_r = 4.3, tan\delta = 0.025$	Uniquely combines broadband circular polarization with low RCS, utilizing orthogonal metasurface elements; Antennas with inherently good radiation and low-RCS features.
[106]	1.6λ × 1.6λ / 0.4λ × 0.4λ at 6 GHz	5.0 GHz, 5.4 GHz, 6.0 GHz, and 6.3 GHz	~13 dBi & not mentioned	Linear, not reconfigurable, measurement + simulation	Dielectric, $\varepsilon_r = 2.65, tan\delta = 0.001$, thickness 3 mm	Utilizes phase cancellation for wideband RCS reduction, enhancing radiation and scattering performance simultaneously; Multiband multiple usage

miniaturization. Optimizing unit cell design and integrating novel materials can lead to metantennas that surpass traditional antenna capabilities.

- *Miniaturization for Wearable and IoT Applications:* With the increasing demand for compact wireless devices, metantennas can be further miniaturized to facilitate integration into wearables, IoT devices, and portable communication systems. Developing even smaller and more efficient metantennas will be essential for next-generation technology.
- *Reconfigurable Metasurfaces for Dynamic Applications:* The ability to dynamically reconfigure metasurfaces will be crucial for applications such as adaptive beam steering and real-time polarization control. Future advancements should explore the integration of liquid crystals, tunable materials, and programmable metasurfaces to achieve greater flexibility. Additionally, rapid optimization techniques using genetic algorithms and machine learning will play a key role in designing adaptive metantennas.
- *Exploring Nonlinear Metasurfaces for Frequency Generation:* Nonlinear metasurfaces can be employed to generate new frequencies and enable nonlinear optical effects, expanding the functionality of metantennas. Future research should focus on integrating these advanced properties to develop multifunctional and frequency-agile antenna systems.
- *Integration with Emerging Technologies:* Metantennas can be combined with RFID, sensors, and smart surfaces to develop next-generation intelligent communication and sensing systems. Future developments may focus on seamless integration with other technologies, enabling metantennas to serve as key components in wireless networks, smart environments, and autonomous systems.

To fully unlock the potential of metantennas, several key challenges must be addressed, including the development of efficient and scalable fabrication techniques, seamless integration with other components and systems, and performance optimization for specific applications. By overcoming these

TABLE 8. Comparison of Leaky wave Metantenna design based on various parameters.

Ref.	Overall Size/Unit Cell Dimension	Bandwidth /Operating Frequency	Gain (dBi) & Efficiency	Polarization Reconfigurability & Validation Method	Substrate Material	Novelty and Application
[108]	Model 1: $0.253\lambda_0 \times 0.059\lambda_0$ Model 2: $0.175\lambda_0 \times 0.059\lambda_0$ / $0.16\lambda_0 \times 0.16\lambda_0$	Model 1: 4.8-7.9 GHz / 5.85 GHz Model 2: 4.8-8 GHz / 5.85 GHz	6.7-7.7 dBi & over 90% radiation efficiency	Linear, not mentioned, measurement + simulation	Dielectric, $\varepsilon_r = 3.55, tan\delta = 0.0057$, thickness = $0.0297\lambda_0$	Uses alumina ceramic to enhance impedance matching and radiation efficiency, enabling stable wide beam-scanning; Wider beam-scanning
[109]	$9.04\lambda_0 \times 6.85\lambda_0$ / $0.57\lambda_0 \times 0.43\lambda_0$	20.55 GHz	Not mentioned	Dual, reconfigurable, measurement + simulation	Rogers RO3003, $\varepsilon_r = 3, tan\delta = 0.001$, thickness= $0.104\lambda_0$	Uses quasi-bound states in the continuum, enabling customizable radiation control via tailored symmetry manipulation; Wireless power transfer, sensing, communication, imaging, and radar
[111]	Antenna: $4.4\lambda_0 \times 0.5\lambda_0$; Metasurface: $5.33\lambda_0 \times 0.5\lambda_0$; Unit cell: $0.13\lambda_0 \times 0.13\lambda_0$	9.5-10.45 GHz / 10 GHz	~9 dBi & 83% radiation efficiency	Linear, not mentioned, measurement + simulation	Rogers 5880, $\varepsilon_r = 2.2, tan\delta = 0.0009$, thickness = $0.017\lambda_0$; Rogers RO3003, $\varepsilon_r = 3, tan\delta = 0.0013$, thickness= $0.051\lambda_0$	Uses Huygens' metasurfaces to reduce beam squinting in leaky-wave antennas by up to 50%; Building simple, low-profile, and low-cost communication systems
[112]	Model 1: $0.75\lambda_0 \times 0.75\lambda_0$ Model 2: $0.72\lambda_0 \times 0.57\lambda_0$	Model 1: 5.45 GHz; Model 2: 5.51 GHz	~10.3 dBi & over 94% radiation efficiency	Linear, not mentioned, measurement + simulation	Rogers RO4003C, $\varepsilon_r = 3.55, tan\delta = 0.0027$, thickness= $0.043\lambda_0$ (Model 1), $0.06\lambda_0$ (Model 2)	Uses an L-probe feed to simultaneously excite TM leaky wave and TE surface wave resonances, achieving wide impedance bandwidth, high front-to-back ratio, and efficient radiation; Wireless applications
[113]	$1.84\lambda_0 \times 1.84\lambda_0$ / Largest unit cell: $0.22\lambda_0 \times 0.22\lambda_0$	0.316 THz	~13 dBi & ~75% radiation efficiency	Not mentioned, not reconfigurable, simulation only	GaAs, $\varepsilon_r = 12.9$, thickness= $0.169\lambda_0$	Optimizing performance by varying substrate thickness to achieve a balance between high gain and wide bandwidth in the THz range; Applications in the THz frequency range
[114]	Unit cell period: $0.2\lambda_0$	1 THz	14.3-29 dB & above 90%	Linear, not mentioned, simulation only	Zeonor, $\varepsilon_r = 2.3, tan\delta = 0.001$, thickness= $0.33\lambda_0$	Uses a fishnet-like unit cell, which offers high efficiency, low impedance, and tunable properties for enhanced reconfigurability; Fabry-Perot cavity leaky-wave antennas for efficient THz radiating devices
[115]	Unit cell: $0.17\lambda_0 \times 0.105\lambda_0$	20 GHz	11-12 dBi & above 80%	Linear, not reconfigurable, measurement + simulation	Rogers RO3010, $\varepsilon_r = 12.94$, thickness = $0.085\lambda_0$; Rogers RO2929 bondply, $\varepsilon_r = 2.94$, thickness = $0.0034\lambda_0$	Enables arbitrary control of radiation parameters, suppression of the open-stopband effect, and the achievement of broadside radiation without degradation; Millimeter-wave applications, radar, sensing, and communication systems

challenges and exploring future advancements, metantennas can revolutionize wireless communication, sensing, and beyond. The future of metantennas looks highly promising, with expected progress in enhanced performance, seamless integration with emerging technologies, miniaturization, cost-effectiveness, reconfigurability, and nonlinear metasurfaces. Furthermore, advancements in Artificial Intelligence (AI) and Machine Learning (ML) could play a crucial role in optimizing metantenna design and adaptive beamforming, further enhancing their capabilities in next-generation communication systems.

V. EMERGING MATERIALS AND TECHNOLOGIES FOR METANTENNA DESIGN

Metantennas have seen significant advancements through the incorporation of novel materials and technologies, including

TABLE 9. Comparison of performance enhancer Metantenna design based on various parameters.

Ref.	Overall Size/Unit Cell Dimension	Bandwidth /Operating Frequency	Gain (dBi) & Efficiency	Polarization Reconfigurability & Validation Method	Substrate Material	Novelty and Application
[116]	$0.58\lambda_0 \times 0.58\lambda_0$ / $0.031\lambda_0 \times 0.031\lambda_0$	3.65 GHz	5.15-5.25 dBi & 70% aperture efficiency	Dual, reconfigurable, measurement + simulation	FR4, $\varepsilon_r = 4.4, tan\delta = 0.02$, thickness = $0.04\lambda_0$	Achieves 46% size reduction, reconfigurability using two PIN diodes; Wireless communication systems, radar systems, and satellite communication systems
[118]	Unit cell: $0.8\lambda_0 \times 0.8\lambda_0$	1.4-2.2 GHz / 2 GHz	~1.3 dB & 22.3% radiation efficiency	Not mentioned, not mentioned, measurement + simulation	Soda-lime glass, $\varepsilon_r = 6.58, tan\delta = 0.018$, thickness = $0.029\lambda_0$ (upper), $0.007\lambda_0$ (lower)	Uses Indium Tin Oxide, achieving over 50% optical transmittivity and broadband RF energy harvesting; Solar panels for realizing efficient RF/solar hybrid energy harvesting
[119]	$1.68\lambda_0 \times 1.68\lambda_0$ / $0.18\lambda_0 \times 0.18\lambda_0$	8.87-9.78 GHz / 9 GHz	15.7 dBi & ~62%	Linear, not reconfigurable, measurement + simulation	Rogers 5880, $\varepsilon_r = 2.2, tan\delta = 0.0009$, thickness = $0.06\lambda_0$ and $0.09\lambda_0$	Integration of low sidelobe radiation and low in-band co-polarized scattering using characteristic mode analysis; Indoor communication, wireless power transmission, smart field control
[120]	Unit cell: $0.51\lambda_0 \times 0.51\lambda_0$	27-31 GHz / 29 GHz	22.7 dBi & 22.7 dBic aperture efficiency	Circular, not mentioned, measurement + simulation	Rogers RO4003C, $\varepsilon_r = 3.55, tan\delta = 0.0027$	Introduction of metantennas reduces the use of phase shifters; Next-generation satellite and radar systems, as well as 5G Advanced and future 6G wireless communication systems
[121]	Unit cell: $0.72\lambda_0 \times 0.72\lambda_0$	2.025-2.29 GHz / 2.15 GHz	7.4-8 dBic & ~96% aperture efficiency	Circular, reconfigurable, simulation only	Sub.1: Rogers TMM3, $\varepsilon_r = 3.46, tan\delta = 0.002$, thickness = $0.05\lambda_0$; Sub.2 & Sub.4: Rogers TMM4, $\varepsilon_r = 4.5, tan\delta = 0.002$, thickness = $0.0036\lambda_0$ & $0.014\lambda_0$; Sub.3: Rogers RO4450B, $\varepsilon_r = 3.54, tan\delta = 0.004$	Significant performance enhancements in aperture efficiency and circular polarization; Nanosatellite: earth observation, meteorology, internet of things, and deep space

liquid crystals, liquid metals, and 3D printing. These innovations have led to improved performance, reconfigurability, and miniaturization of antenna designs.

A. LIQUID CRYSTALS IN METANTENNAS

Phase Shifting and Beam Steering: Liquid crystals are utilized in metantennas primarily for their ability to adjust the phase of electromagnetic waves, which is crucial for electronically steered phased arrays and metamaterial-based antennas. This adjustment is achieved through various liquid crystal-based phase shifters and is essential for controlling the refractive index around antenna elements to influence resonance [34], [134], [135].

Reconfigurable Metasurfaces: Liquid crystals enable the development of electronically tunable metasurfaces, which are high impedance surfaces that can dynamically alter their reflection phase. This capability is particularly useful for creating large, dual-polarized, beam-steering metantennas suitable for millimeter-wave applications [136], [137].

Dual-Tuned Modes: Advanced designs incorporate dual-tuned modes of liquid crystal materials, allowing for expanded beam-steering ranges and enhanced flexibility in metantenna design. These designs use composite right/left-handed transmission lines to achieve continuous electronic beam-steering across a broad frequency band [138].

B. LIQUID METALS IN METANTENNAS

Liquid metals offer significant advantages for flexibility and adaptiveness in metantenna designs. They allow for the creation of reconfigurable antennas that can alter their properties by changing the arrangement of the liquid metal within microfluidic channels. This approach enhances functionality, enabling the metantennas to be stretchable or wearable without sacrificing performance [35]. Additionally, liquid metal metantennas can be developed to effectively

TABLE 10. Comparison of End-fire Metantenna design based on various parameters.

Ref.	Overall Size/Unit Cell Dimension	Bandwidth /Operating Frequency	Gain (dBi) & Efficiency	Polarization Reconfigurability & Validation Method	Substrate Material	Novelty and Application
[122]	7.77λ × 3.33λ × 0.28λ at 10 GHz	3.78-18.54 GHz	~5.73-16.2 dBi & not mentioned	Linear, not mentioned, measurement + simulation	Antenna: Teflon, $\varepsilon_r = 2.2, tan\delta = 0.0002$; Ceramic, $\varepsilon_r = 25$, thickness = 0.17λ at 10 GHz. Metasurface: Taconic TLY, $\varepsilon_r = 2.2, tan\delta = 0.0009$, thickness = 0.017λ at 10 GHz	Integration of a metasurface and a blind-filled cylindrical hole to enhance the radiation pattern and bandwidth; Aerospace and defense: communication, radar, and sensing
[123]	Unit cell: 0.17λ × 0.22λ at 28 GHz	28-37 GHz	12-18.1 dBi & not mentioned	Linear, not mentioned, simulation only	Rogers 5880, $\varepsilon_r = 2.2, tan\delta = 0.0009$, thickness = 0.14λ at 28 GHz	Use of a double-layer metasurface enhances gain performance over a wide frequency range; Millimeter-wave applications for end-fire radiation
[124]	Lens radius $3.28\lambda_0$ / $0.14\lambda_0 \times 0.14\lambda_0$	13 GHz	~15 dBi & ~75% total efficiency	Linear, not mentioned, simulation only	Rogers RO3210, $\varepsilon_r = 10.2, tan\delta = 0.0027$, thickness = $0.03\lambda_0$	Design of metantenna with variable surface impedance through size-varying circular patches; Pencil beam radiation, new communication antennas, and sensor
[125]	Metasurface lens radius $1.33\lambda_0$ / $0.15\lambda_0 \times 0.11\lambda_0$	10 GHz	Not mentioned	Not mentioned, not reconfigurable, simulation only	Dielectric, $\varepsilon_r = 2.2$, thickness = $0.033\lambda_0$	Enables independent refractive index control along two optical axes; Collimating lights, radar antennas, and wide-angle cameras
[126]	Lens radius 1.91λ / 0.14λ × 0.14λ at 10 GHz	8-12 GHz	14-15 dBi & not mentioned	Linear, not mentioned, measurement + simulation	Rogers 5880, $\varepsilon_r = 2.2, tan\delta = 0.0009$, thickness = 0.053λ at 10 GHz	Uses a planar metamaterial-based Luneburg lens, enabling efficient beam scanning from −60° to +60°; Beam-scanning with a coverage of up to 120°

TABLE 11. Working principles, Equivalent circuit models, and performance impact of metasurface unit cells.

Ref.	Unit Cell Type	Working Principle	Equivalent Circuit Model (ECM)	Impact on Performance
[44], [127]	Resonant Patch/Slot	Phase control via resonance of metallic inclusions (patches, rings, slots, crosses)	LC resonator (C = gap capacitance, L = current path inductance)	Provides 360° phase shift; compact, high gain; narrow bandwidth due to high Q-factor resonance
[128]	AMC / High-Impedance Surface	In-phase reflection at resonance (artificial magnetic conductor behavior)	Parallel LC (C = patch gap, L = via + substrate thickness)	Enables low-profile antennas; suppresses surface waves; band-limited around AMC frequency
[85], [129]	Huygens' Unit Cell	Balanced electric and magnetic dipoles for reflectionless transmission	Matched admittance/impedance sheets	Achieves unity transmission, broadband, and efficient phase control
[130], [131]	PB-Phase Unit Cell	Rotation angle imparts phase ($\phi = \pm 2\psi$); polarization-dependent	Polarization transformation (Jones matrix)	Ideal for CP/OAM beams; simple implementation; bandwidth limited by conversion efficiency
[132]	Bianisotropic / Omega-Type	Magnetoelectric coupling allows asymmetric wave control	Generalized Z-matrix with off-diagonal coupling terms	Enables angularly robust reflection/refraction; asymmetric transmission
[133]	Absorber (MIM / Salisbury)	Impedance-matched lossy metasurface absorbs incident energy	RLC-loaded resonant layer backed by ground plane	High absorption for stealth/RCS reduction; narrowband unless multi-layered
[108]	CRLH TL	Gap capacitance + stub inductance forms a balanced CRLH line	Series C (gap), shunt L (stub), ACB-enhanced C	Miniaturization, >90% radiation efficiency, wide scanning (−70° to +69°), improved gain (7.7 dBi)

manage radar cross-section, making them suitable for stealth applications [139].

Recent studies have also highlighted the ability of liquid metals to enable independent modulation of antenna units,

forming arrays that can achieve flexible beam steering capabilities. This flexibility is vital for applications in advanced communication networks, particularly during dynamic operational conditions [138].

C. 3D PRINTING IN META-ANTENNA FABRICATION

3D printing technologies are revolutionizing the fabrication of metantennas by allowing the creation of complex geometries and structures that are difficult or impossible to achieve with traditional manufacturing methods. This additive manufacturing process not only enables the integration of multiple materials with varying electromagnetic properties but also facilitates speed, cost-effectiveness, and design flexibility [33]. Researchers are exploring various printing techniques to manufacture antennas with specific performance characteristics, such as enhanced gain and bandwidth, by varying layer compositions and structures during the printing process. Liquid metals, such as gallium-based alloys, are used in the fabrication of 3D metantennas. These metals can be vacuum-filled into 3D printed cavities, allowing for the creation of complex, conductive geometries without defects. This method supports rapid prototyping and the development of reconfigurable metantennas, as the liquid metal can be manipulated to alter the antenna's properties [140].

Moreover, 3D printing allows for the incorporation of metamaterials that can impart unique electromagnetic responses, aiding in compact designs that maintain high performance despite size reductions [141]. The ability to create complex internal structures could lead to innovations in antenna designs that efficiently utilize space while maximizing functionality.

VI. CONCLUSION

The emergence of metasurfaces has revolutionized antenna design, driving significant advancements in performance, integration, and functionality. These developments have had a twofold impact. First, the incorporation of functional metasurfaces has notably enhanced antenna performance, encompassing improvements in gain (directivity), expanded operating bandwidth, increased aperture efficiency, reduced profile or volume, lowered RCS, controlled radiation patterns, among other factors. Second, metasurfaces have evolved into primary radiating apertures, where metantennas, when integrated with feeding structures, provide superior performance and additional functionalities. Unlike conventional supplementary elements, metasurfaces actively couple, transmit, and decouple electromagnetic waves, enabling highly integrated and reconfigurable antenna architectures. The ability of metasurfaces to manipulate electromagnetic waves introduces a new level of technical competence, making them highly relevant across industries such as telecommunications, transportation, and defense. As the demand for compact and adaptive antennas grows, metasurface-based designs offer a transformative approach. While their design can be complex and resource-intensive, rapid advancements in computational techniques, including machine learning, genetic algorithms, and optimization methods, are helping to streamline their development. Additionally, innovations in material science, such as liquid crystal-based tunable metasurfaces and 3D-printed structures, are expanding their adaptability for next-generation applications.

This article presents a comprehensive overview of metantennas, including their first-ever detailed classification based on operation, generation, and function. It explores various metantenna types, their advantages and challenges, and provides a comparative performance analysis. By offering valuable insights into their design and applications, this work serves as a critical reference for researchers striving to develop compact, high-performance metantennas for diverse applications. Looking ahead, metantennas are poised to play a crucial role in the evolution of wireless communication, sensing, and beyond. Ongoing research continues to refine their capabilities, improve efficiency, and expand their applications. Furthermore, advancements in Artificial Intelligence (AI) and novel materials will be instrumental in shaping the next generation of metantennas, enabling unparalleled adaptability and integration with intelligent systems. With continuous innovations in reconfigurability, miniaturization, and smart antenna technologies, metantennas hold immense potential to drive unprecedented advancements in next-generation electromagnetic systems.

ACKNOWLEDGMENT

A part of Fig. 1 is custom-created with the assistance of Freepik, a paid AI-based creative suite, and has been further modified by the authors to suit the context of this work.

REFERENCES

[1] D. R. Smith, D. C. Vier, T. Koschny, and C. M. Soukoulis, "Electromagnetic parameter retrieval from inhomogeneous metamaterials," *Phys. Rev. E, Stat. Phys. Plasmas Fluids Relat. Interdiscip. Top.*, vol. 71, no. 3, Mar. 2005, Art. no. 036617, doi: 10.1103/physreve.71.036617.

[2] C. Milias, R. B. Andersen, P. I. Lazaridis, Z. D. Zaharis, B. Muhammad, J. T. B. Kristensen, A. Mihovska, and D. D. S. Hermansen, "Metamaterial-inspired antennas: A review of the state of the art and future design challenges," *IEEE Access*, vol. 9, pp. 89846–89865, 2021, doi: 10.1109/ACCESS.2021.3091479.

[3] S. B. Glybovski, S. A. Tretyakov, P. A. Belov, Y. S. Kivshar, and C. R. Simovski, "Metasurfaces: From microwaves to visible," *Phys. Rep.*, vol. 634, pp. 1–72, May 2016, doi: 10.1016/j.physrep.2016.04.004.

[4] N. Yu, P. Genevet, F. Aieta, M. A. Kats, R. Blanchard, G. Aoust, J.-P. Tetienne, Z. Gaburro, and F. Capasso, "Flat optics: Controlling wavefronts with optical antenna metasurfaces," *IEEE J. Sel. Topics Quantum Electron.*, vol. 19, no. 3, pp. 4700423–4700423, May 2013, doi: 10.1109/JSTQE.2013.2241399.

[5] A. M. Patel and A. Grbic, "The effects of spatial dispersion on power flow along a printed-circuit tensor impedance surface," *IEEE Trans. Antennas Propag.*, vol. 62, no. 3, pp. 1464–1469, Mar. 2014, doi: 10.1109/TAP.2013.2294196.

[6] S. Maci, G. Minatti, M. Casaletti, and M. Bosiljevac, "Metasurfing: Addressing waves on impenetrable metasurfaces," *IEEE Antennas Wireless Propag. Lett.*, vol. 10, pp. 1499–1502, 2011, doi: 10.1109/LAWP.2012.2183631.

[7] A. Tellechea Pereda, F. Caminita, E. Martini, I. Ederra, J. C. Iriarte, R. Gonzalo, and S. Maci, "Dual circularly polarized broadside beam metasurface antenna," *IEEE Trans. Antennas Propag.*, vol. 64, no. 7, pp. 2944–2953, Jul. 2016, doi: 10.1109/TAP.2016.2562662.

[8] S. Pandi, C. A. Balanis, and C. R. Birtcher, "Design of scalar impedance holographic metasurfaces for antenna beam formation with desired polarization," *IEEE Trans. Antennas Propag.*, vol. 63, no. 7, pp. 3016–3024, Jul. 2015, doi: 10.1109/TAP.2015.2426832.

[9] M. Faenzi, F. Caminita, E. Martini, P. De Vita, G. Minatti, M. Sabbadini, and S. Maci, "Realization and measurement of broadside beam modulated metasurface antennas," *IEEE Antennas Wireless Propag. Lett.*, vol. 15, pp. 610–613, 2016, doi: 10.1109/LAWP.2015.2463108.

[10] G. Minatti, M. Faenzi, E. Martini, F. Caminita, P. De Vita, D. González-Ovejero, M. Sabbadini, and S. Maci, "Modulated metasurface antennas for space: Synthesis, analysis and realizations," *IEEE Trans. Antennas Propag.*, vol. 63, no. 4, pp. 1288–1300, Apr. 2015, doi: 10.1109/TAP.2014.2377718.

[11] A. M. Patel and A. Grbic, "A printed leaky-wave antenna based on a sinusoidally-modulated reactance surface," *IEEE Trans. Antennas Propag.*, vol. 59, no. 6, pp. 2087–2096, Jun. 2011, doi: 10.1109/TAP.2011.2143668.

[12] G. Minatti, F. Caminita, M. Casaletti, and S. Maci, "Spiral leaky-wave antennas based on modulated surface impedance," *IEEE Trans. Antennas Propag.*, vol. 59, no. 12, pp. 4436–4444, Dec. 2011, doi: 10.1109/TAP.2011.2165691.

[13] D. Gonzalez-Ovejero, T. J. Reck, C. D. Jung-Kubiak, M. Alonso-DelPino, and G. Chattopadhyay, "A class of silicon micromachined metasurface for the design of high-gain terahertz antennas," in *Proc. IEEE Int. Symp. Antennas Propag. (APSURSI)*, Jun. 2016, pp. 1191–1192, doi: 10.1109/APS.2016.7696303.

[14] A. Li, S. Singh, and D. Sievenpiper, "Metasurfaces and their applications," *Nanophotonics*, vol. 7, no. 6, pp. 989–1011, Jun. 2018, doi: 10.1515/nanoph-2017-0120.

[15] W. Li, Q. Ma, C. Liu, Y. Zhang, X. Wu, J. Wang, S. Gao, T. Qiu, T. Liu, Q. Xiao, J. Wei, T. T. Gu, Z. Zhou, F. Li, Q. Cheng, L. Li, W. Tang, and T. J. Cui, "Intelligent metasurface system for automatic tracking of moving targets and wireless communications based on computer vision," *Nature Commun.*, vol. 14, no. 1, p. 989, Feb. 2023, doi: 10.1038/s41467-023-36645-3.

[16] M. Faenzi, G. Minatti, D. González-Ovejero, F. Caminita, E. Martini, C. D. Giovampaola, and S. Maci, "Metasurface antennas: New models, applications and realizations," *Sci. Rep.*, vol. 9, no. 1, Jul. 2019, Art. no. 1, doi: 10.1038/s41598-019-46522-z.

[17] J. Wang, Y. Li, Z. H. Jiang, T. Shi, M.-C. Tang, Z. Zhou, Z. N. Chen, and C.-W. Qiu, "Metantenna: When metasurface meets antenna again," *IEEE Trans. Antennas Propag.*, vol. 68, no. 3, pp. 1332–1347, Mar. 2020, doi: 10.1109/TAP.2020.2969246.

[18] Z. N. Chen, X. Qing, Y. Su, and R. Xu, "Toward metantennas: Metamaterial-based antennas for wireless communications," *IEEE Commun. Mag.*, vol. 61, no. 11, pp. 160–165, Nov. 2023, doi: 10.1109/MCOM.001.2300070.

[19] G. Minatti, F. Caminita, E. Martini, and S. Maci, "Flat optics for leaky-waves on modulated metasurfaces: Adiabatic floquet-wave analysis," *IEEE Trans. Antennas Propag.*, vol. 64, no. 9, pp. 3896–3906, Sep. 2016, doi: 10.1109/TAP.2016.2590559.

[20] S. S. Bukhari, J. Vardaxoglou, and W. Whittow, "A metasurfaces review: Definitions and applications," *Appl. Sci.*, vol. 9, no. 13, p. 2727, Jul. 2019, doi: 10.3390/app9132727.

[21] M. Hussain, W. A. Awan, M. S. Alzaidi, N. Hussain, E. M. Ali, and F. Falcone, "Metamaterials and their application in the performance enhancement of reconfigurable antennas: A review," *Micromachines*, vol. 14, no. 2, p. 349, Jan. 2023, doi: 10.3390/mi14020349.

[22] C. A. Balanis, *Antenna Theory: Analysis and Design*. Hoboken, NJ, USA: Wiley, 2012.

[23] M. Yan, J. Wang, H. Ma, M. Feng, Y. Pang, S. Qu, J. Zhang, and L. Zheng, "A tri-band, highly selective, bandpass FSS using cascaded multilayer loop arrays," *IEEE Trans. Antennas Propag.*, vol. 64, no. 5, pp. 2046–2049, May 2016, doi: 10.1109/TAP.2016.2536175.

[24] C. R. Simovski, P. de Maagt, and I. V. Melchakova, "High-impedance surfaces having stable resonance with respect to polarization and incidence angle," *IEEE Trans. Antennas Propag.*, vol. 53, no. 3, pp. 908–914, Mar. 2005, doi: 10.1109/TAP.2004.842598.

[25] A. S. Barlevy and Y. Rahmat-Samii, "Characterization of electromagnetic band-gaps composed of multiple periodic tripods with interconnecting vias: Concept, analysis, and design," *IEEE Trans. Antennas Propag.*, vol. 49, no. 3, pp. 343–353, Mar. 2001, doi: 10.1109/8.918607.

[26] C. L. Holloway, E. F. Kuester, J. A. Gordon, J. O'Hara, J. Booth, and D. R. Smith, "An overview of the theory and applications of metasurfaces: The two-dimensional equivalents of metamaterials," *IEEE Antennas Propag. Mag.*, vol. 54, no. 2, pp. 10–35, Apr. 2012, doi: 10.1109/MAP.2012.6230714.

[27] J. A. Gordon, C. L. Holloway, and A. Dienstfrey, "A physical explanation of angle-independent reflection and transmission properties of metafilms/metasurfaces," *IEEE Antennas Wireless Propag. Lett.*, vol. 8, pp. 1127–1130, 2009, doi: 10.1109/LAWP.2009.2033216.

[28] C. L. Holloway, E. F. Kuester, and A. Dienstfrey, "Characterizing metasurfaces/metafilms: The connection between surface susceptibilities and effective material properties," *IEEE Antennas Wireless Propag. Lett.*, vol. 10, pp. 1507–1511, 2011, doi: 10.1109/LAWP.2011.2182591.

[29] Z. Yu, M. Li, Z. Xing, H. Gao, Z. Liu, S. Pu, H. Mao, H. Cai, Q. Ma, W. Ren, J. Zhu, and C. Zhang, "Genetic algorithm assisted meta-atom design for high-performance metasurface optics," *Opto-Electron. Sci.*, vol. 3, no. 9, Sep. 2024, Art. no. 240016, doi: 10.29026/oes.2024.240016.

[30] S. Jafar-Zanjani, S. Inampudi, and H. Mosallaei, "Adaptive genetic algorithm for optical metasurfaces design," *Sci. Rep.*, vol. 8, no. 1, p. 11040, Jul. 2018, doi: 10.1038/s41598-018-29275-z.

[31] G. Yang, Q. Xiao, Z. Zhang, Z. Yu, X. Wang, and Q. Lu, "Exploring AI in metasurface structures with forward and inverse design," *IScience*, vol. 28, no. 3, Mar. 2025, Art. no. 111995, doi: 10.1016/j.isci.2025.111995.

[32] S. Koziel, A. Pietrenko-Dabrowska, and L. Leifsson, "Antenna optimization using machine learning with reduced-dimensionality surrogates," *Sci. Rep.*, vol. 14, no. 1, p. 21567, Sep. 2024, doi: 10.1038/s41598-024-72478-w.

[33] T. Whittaker, S. Zhang, A. Powell, C. J. Stevens, J. Y. C. Vardaxoglou, and W. Whittow, "3D printing materials and techniques for antennas and metamaterials: A survey of the latest advances," *IEEE Antennas Propag. Mag.*, vol. 65, no. 3, pp. 10–20, Jun. 2023, doi: 10.1109/MAP.2022.3229298.

[34] T.-L. Ting, "Technology of liquid crystal based antenna [invited]," *Opt. Exp.*, vol. 27, no. 12, pp. 17138–17153, Jun. 2019, doi: 10.1364/oe.27.017138.

[35] K. N. Paracha, A. D. Butt, A. S. Alghamdi, S. A. Babale, and P. J. Soh, "Liquid metal antennas: Materials, fabrication and applications," *Sensors*, vol. 20, no. 1, p. 177, Dec. 2019, doi: 10.3390/s20010177.

[36] G.-P. Gao, C. Yang, B. Hu, R.-F. Zhang, and S.-F. Wang, "A wearable PIFA with an all-textile metasurface for 5 GHz WBAN applications," *IEEE Antennas Wireless Propag. Lett.*, vol. 18, pp. 288–292, 2019, doi: 10.1109/LAWP.2018.2889117.

[37] L. Stefanini, A. Rech, D. Ramaccia, S. Tomasin, A. Toscano, F. Moretto, and F. Bilotti, "Multibeam scanning antenna system based on beamforming metasurface for fast 5G NR initial access," *IEEE Access*, vol. 10, pp. 65982–65995, 2022, doi: 10.1109/ACCESS.2022.3183754.

[38] A. Welkie, L. Shangguan, J. Gummeson, W. Hu, and K. Jamieson, "Programmable radio environments for smart spaces," in *Proc. 16th ACM Workshop Hot Topics Netw.* New York, NY, USA: Association for Computing Machinery, Nov. 2017, pp. 36–42, doi: 10.1145/3152434.3152456.

[39] C. Liaskos, S. Nie, A. Tsioliaridou, A. Pitsillides, S. Ioannidis, and I. Akyildiz, "Realizing wireless communication through software-defined hypersurface environments," in *Proc. IEEE 19th Int. Symp. World Wireless, Mobile Multimedia Netw. (WoWMoM)*, Jun. 2018, pp. 14–15, doi: 10.1109/WOWMOM.2018.8449754.

[40] E. Basar, M. Di Renzo, J. De Rosny, M. Debbah, M.-S. Alouini, and R. Zhang, "Wireless communications through reconfigurable intelligent surfaces," *IEEE Access*, vol. 7, pp. 116753–116773, 2019, doi: 10.1109/ACCESS.2019.2935192.

[41] O. Quevedo-Teruel and Q. Chen, "Classification and opportunities of metasurfaces for antenna designs," in *Proc. Int. Symp. Antennas Propag. (ISAP)*, Oct. 2021, pp. 1–2, doi: 10.23919/ISAP47258.2021.9614437.

[42] A. Grbic and S. Maci, "EM metasurfaces [guest editorial]," *IEEE Antennas Propag. Mag.*, vol. 64, no. 4, pp. 16–22, Aug. 2022, doi: 10.1109/MAP.2022.3178924.

[43] C. G. M. Ryan, M. R. Chaharmir, J. Shaker, J. R. Bray, Y. M. M. Antar, and A. Ittipiboon, "A wideband transmitarray using dual-resonant double square rings," *IEEE Trans. Antennas Propag.*, vol. 58, no. 5, pp. 1486–1493, May 2010, doi: 10.1109/TAP.2010.2044356.

[44] J. Huang and J. A. Encinar, *Reflectarray Antennas*. Hoboken, NJ, USA: Wiley, 2007.

[45] D. M. Pozar and T. A. Metzler, "Analysis of a reflectarray antenna using microstrip patches of variable size," *Electron. Lett.*, vol. 29, no. 8, pp. 657–658, Apr. 1993, doi: 10.1049/el:19930440.

[46] M. Feng, Y. Li, J. Wang, Q. Zheng, S. Sui, C. Wang, H. Chen, H. Ma, S. Qu, and J. Zhang, "Ultra-wideband and high-efficiency transparent coding metasurface," *Appl. Phys. A, Solids Surf.*, vol. 124, no. 9, p. 630, Aug. 2018, doi: 10.1007/s00339-018-2048-9.

[47] Y. Li, J. Zhang, S. Qu, J. Wang, Y. Pang, and Z. Xu, "Ultra-wideband, high-efficiency beam steering based on phase gradient metasurfaces," *J. Electromagn. Waves Appl.*, vol. 29, no. 16, pp. 2163–2170, Nov. 2015, doi: 10.1080/09205071.2015.1078747.

[48] Y. Han, J. Zhang, Y. Li, J. Wang, S. Qu, H. Yuan, and J. Yu, "Miniaturized-element offset-feed planar reflector antennas based on metasurfaces," *IEEE Antennas Wireless Propag. Lett.*, vol. 16, pp. 282–285, 2017, doi: 10.1109/LAWP.2016.2572878.

[49] H.-X. Xu, S. Tang, G.-M. Wang, T. Cai, W. Huang, Q. He, S. Sun, and L. Zhou, "Multifunctional microstrip array combining a linear polarizer and focusing metasurface," *IEEE Trans. Antennas Propag.*, vol. 64, no. 8, pp. 3676–3682, Aug. 2016, doi: 10.1109/TAP.2016.2565742.

[50] Y. B. Li, L. L. Li, B. B. Xu, W. Wu, R. Y. Wu, X. Wan, Q. Cheng, and T. J. Cui, "Transmission-type 2-bit programmable metasurface for single-sensor and single-frequency microwave imaging," *Sci. Rep.*, vol. 6, no. 1, Mar. 2016, Art. no. 1, doi: 10.1038/srep23731.

[51] X. Wan, M. Q. Qi, T. Y. Chen, and T. J. Cui, "Field-programmable beam reconfiguring based on digitally-controlled coding metasurface," *Sci. Rep.*, vol. 6, no. 1, Feb. 2016, Art. no. 1, doi: 10.1038/srep20663.

[52] J.-B. Yu, H. Ma, J.-F. Wang, Y.-F. Li, M.-D. Feng, and S.-B. Qu, "High-efficiency wideband flat focusing reflector mediated by metasurfaces," *Chin. Phys. B*, vol. 24, no. 9, Sep. 2015, Art. no. 098102, doi: 10.1088/1674-1056/24/9/098102.

[53] K. Chen, Z. Yang, Y. Feng, B. Zhu, J. Zhao, and T. Jiang, "Improving microwave antenna gain and bandwidth with phase compensation metasurface," *AIP Adv.*, vol. 5, no. 6, Jun. 2015, Art. no. 067152, doi: 10.1063/1.4923195.

[54] S. S. Syed Nasser, W. Liu, and Z. N. Chen, "Wide bandwidth and enhanced gain of a low-profile dipole antenna achieved by integrated suspended metasurface," *IEEE Trans. Antennas Propag.*, vol. 66, no. 3, pp. 1540–1544, Mar. 2018, doi: 10.1109/TAP.2018.2790161.

[55] N. Nasimuddin, Z. N. Chen, and X. Qing, "Bandwidth enhancement of a single-feed circularly polarized antenna using a metasurface: Metamaterial-based wideband CP rectangular microstrip antenna," *IEEE Antennas Propag. Mag.*, vol. 58, no. 2, pp. 39–46, Apr. 2016, doi: 10.1109/MAP.2016.2520257.

[56] A. Epstein, J. P. S. Wong, and G. V. Eleftheriades, "Cavity-excited Huygens' metasurface antennas for near-unity aperture illumination efficiency from arbitrarily large apertures," *Nature Commun.*, vol. 7, no. 1, Jan. 2016, Art. no. 1, doi: 10.1038/ncomms10360.

[57] M. E. Badawe, T. S. Almoneef, and O. M. Ramahi, "A true metasurface antenna," *Sci. Rep.*, vol. 6, no. 1, Jan. 2016, Art. no. 1, doi: 10.1038/srep19268.

[58] H. Chen, H. Ma, Y. Li, J. Wang, Y. Han, M. Yan, and S. Qu, "Wideband frequency scanning spoof surface plasmon polariton planar antenna based on transmissive phase gradient metasurface," *IEEE Antennas Wireless Propag. Lett.*, vol. 17, pp. 463–467, 2018, doi: 10.1109/LAWP.2018.2795341.

[59] Y. Fan, J. Wang, H. Ma, J. Zhang, D. Feng, M. Feng, and S. Qu, "In-plane feed antennas based on phase gradient metasurface," *IEEE Trans. Antennas Propag.*, vol. 64, no. 9, pp. 3760–3765, Sep. 2016, doi: 10.1109/TAP.2016.2583472.

[60] Z. N. Chen, D. Liu, H. Nakano, X. Qing, and T. Zwick, *Handbook of Antenna Technologies*. Singapore: Springer, 2016, doi: 10.1007/978-981-4560-44-3.

[61] O. Yurduseven and D. R. Smith, "Dual-polarization printed holographic multibeam metasurface antenna," *IEEE Antennas Wireless Propag. Lett.*, vol. 16, pp. 2738–2741, 2017, doi: 10.1109/LAWP.2017.2743710.

[62] O. Yurduseven, C. Lee, D. González-Ovejero, M. Ettorre, R. Sauleau, G. Chattopadhyay, V. Fusco, and N. Chahat, "Multibeam Si/GaAs holographic metasurface antenna at W-band," *IEEE Trans. Antennas Propag.*, vol. 69, no. 6, pp. 3523–3528, Jun. 2021, doi: 10.1109/TAP.2020.3030898.

[63] M. Sazegar and R. Stevenson, "Holographic metasurface antennas with dynamic beam pointing and polarization control," in *Proc. IEEE Int. Symp. Antennas Propag. North Amer. Radio Sci. Meeting*, Jul. 2020, pp. 1657–1658, doi: 10.1109/IEEECONF35879.2020.9329864.

[64] Z. Li, W. Cui, R. Liu, M. Wang, C. Fan, H. Zheng, and E. Li, "Metantenna design with one-dimensional holographic concept," *Int. J. RF Microw. Comput.-Aided Eng.*, vol. 31, no. 3, Mar. 2021, Art. no. e22536, doi: 10.1002/mmce.22536.

[65] J. Han, L. Li, S. Tian, X. Ma, Q. Feng, H. Liu, Y. Zhao, and G. Liao, "Frequency-diverse holographic metasurface antenna for near-field microwave computational imaging," *Frontiers Mater.*, vol. 8, Oct. 2021, Art. no. 766889. [Online]. Available: https://www.frontiersin.org/articles/10.3389/fmats.2021.766889

[66] J. Wang, S. Qu, H. Ma, Z. Xu, A. Zhang, H. Zhou, H. Chen, and Y. Li, "High-efficiency spoof plasmon polariton coupler mediated by gradient metasurfaces," *Appl. Phys. Lett.*, vol. 101, no. 20, Nov. 2012, Art. no. 201104, doi: 10.1063/1.4767219.

[67] S. Sun, Q. He, S. Xiao, Q. Xu, X. Li, and L. Zhou, "Gradient-index meta-surfaces as a bridge linking propagating waves and surface waves," *Nature Mater.*, vol. 11, no. 5, pp. 426–431, May 2012, doi: 10.1038/nmat3292.

[68] S. Sun, K.-Y. Yang, C.-M. Wang, T.-K. Juan, W. T. Chen, C. Y. Liao, Q. He, S. Xiao, W.-T. Kung, G.-Y. Guo, L. Zhou, and D. P. Tsai, "High-efficiency broadband anomalous reflection by gradient meta-surfaces," *Nano Lett.*, vol. 12, no. 12, pp. 6223–6229, Dec. 2012, doi: 10.1021/nl3032668.

[69] D. R. Smith, O. Yurduseven, L. P. Mancera, P. Bowen, and N. B. Kundtz, "Analysis of a waveguide-fed metasurface antenna," *Phys. Rev. Appl.*, vol. 8, no. 5, Nov. 2017, Art. no. 054048, doi: 10.1103/physrevapplied.8.054048.

[70] Y. Fan, J. Wang, Y. Li, J. Zhang, S. Qu, Y. Han, and H. Chen, "Frequency scanning radiation by decoupling spoof surface plasmon polaritons via phase gradient metasurface," *IEEE Trans. Antennas Propag.*, vol. 66, no. 1, pp. 203–208, Jan. 2018, doi: 10.1109/TAP.2017.2767625.

[71] X. Liu, B. Chen, J. Zhang, W. Li, J. Chen, A. Zhang, and H. Shi, "Frequency-scanning planar antenna based on spoof surface plasmon polariton," *IEEE Antennas Wireless Propag. Lett.*, vol. 16, pp. 165–168, 2017, doi: 10.1109/LAWP.2016.2565603.

[72] Y. B. Li, R. Y. Wu, W. Wu, C. B. Shi, Q. Cheng, and T. J. Cui, "Dual-physics manipulation of electromagnetic waves by system-level design of metasurfaces to reach extreme control of radiation beams," *Adv. Mater. Technol.*, vol. 2, no. 1, Jan. 2017, Art. no. 1600196, doi: 10.1002/admt.201600196.

[73] X. Wan, T. Y. Chen, Q. Zhang, J. Y. Yin, Z. Tao, L. Zhang, X. Q. Chen, Y. B. Li, and T. J. Cui, "Manipulations of dual beams with dual polarizations by full-tensor metasurfaces," *Adv. Opt. Mater.*, vol. 4, no. 10, pp. 1567–1572, Oct. 2016, doi: 10.1002/adom.201600111.

[74] D. González-Ovejero, G. Minatti, G. Chattopadhyay, and S. Maci, "Multibeam by metasurface antennas," *IEEE Trans. Antennas Propag.*, vol. 65, no. 6, pp. 2923–2930, Jun. 2017, doi: 10.1109/TAP.2017.2670622.

[75] Y. B. Li, X. Wan, B. G. Cai, Q. Cheng, and T. J. Cui, "Frequency-controls of electromagnetic multi-beam scanning by metasurfaces," *Sci. Rep.*, vol. 4, no. 1, Nov. 2014, Art. no. 1, doi: 10.1038/srep06921.

[76] X. G. Zhang, W. X. Jiang, H. W. Tian, and T. J. Cui, "Controlling radiation beams by low-profile planar antenna arrays with coding elements," *ACS Omega*, vol. 3, no. 9, pp. 10601–10611, Sep. 2018, doi: 10.1021/acsomega.8b01679.

[77] Z. L. Ma and C. H. Chan, "A novel surface-wave-based high-impedance surface multibeam antenna with full azimuth coverage," *IEEE Trans. Antennas Propag.*, vol. 65, no. 4, pp. 1579–1588, Apr. 2017, doi: 10.1109/TAP.2017.2670320.

[78] M. Chen, M. Kim, A. M. H. Wong, and G. V. Eleftheriades, "Huygens' metasurfaces from microwaves to optics: A review," *Nanophotonics*, vol. 7, no. 6, pp. 1207–1231, Jun. 2018, doi: 10.1515/nanoph-2017-0117.

[79] J. W. Wu, Z. X. Wang, R. Y. Wu, H. Xu, Q. Cheng, and T. J. Cui, "Simple and comprehensive strategy to synthesize Huygens metasurface antenna and verification," *IEEE Trans. Antennas Propag.*, vol. 71, no. 8, pp. 6652–6666, Aug. 2023, doi: 10.1109/TAP.2023.3283062.

[80] C. Z. Ning, L. I. U. Wei, L. I. Teng, L. F. Han, and J. Mei, "Progress in microwave Huygens' metasurface antennas (invited)," *Chin. J. Radio Sci.*, vol. 33, no. 3, pp. 239–255, Jun. 2018, doi: 10.13443/j.cjors.2018050701.

[81] J.-W. Lian, Y.-L. Ban, and Y. J. Guo, "Wideband dual-layer Huygens' metasurface for high-gain multibeam array antennas," *IEEE Trans. Antennas Propag.*, vol. 69, no. 11, pp. 7521–7531, Nov. 2021, doi: 10.1109/TAP.2021.3076669.

[82] C. Xue, Q. Lou, and Z. N. Chen, "Broadband double-layered Huygens' metasurface lens antenna for 5G millimeter-wave systems," *IEEE Trans. Antennas Propag.*, vol. 68, no. 3, pp. 1468–1476, Mar. 2020, doi: 10.1109/TAP.2019.2943440.

[83] A. M. H. Wong and G. V. Eleftheriades, "Perfect anomalous reflection with a bipartite Huygens' metasurface," *Phys. Rev. X*, vol. 8, no. 1, Feb. 2018, Art. no. 011036, doi: 10.1103/physrevx.8.011036.

[84] M. Chen, A. Epstein, and G. V. Eleftheriades, "Design and experimental verification of a passive Huygens' metasurface lens for gain enhancement of frequency-scanning slotted-waveguide antennas," *IEEE Trans. Antennas Propag.*, vol. 67, no. 7, pp. 4678–4692, Jul. 2019, doi: 10.1109/TAP.2019.2911591.

[85] A. Epstein and G. V. Eleftheriades, "Huygens' metasurfaces via the equivalence principle: Design and applications," *J. Opt. Soc. Amer. B, Opt. Phys.*, vol. 33, no. 2, pp. A31–A50, Feb. 2016, doi: 10.1364/josab.33.000a31.

[86] A. Epstein and G. V. Eleftheriades, "Arbitrary power-conserving field transformations with passive lossless omega-type bianisotropic metasurfaces," *IEEE Trans. Antennas Propag.*, vol. 64, no. 9, pp. 3880–3895, Sep. 2016, doi: 10.1109/TAP.2016.2588495.

[87] L. Szymanski, B. O. Raeker, C.-W. Lin, and A. Grbic, "Fundamentals of lossless, reciprocal bianisotropic metasurface design," *Photonics*, vol. 8, no. 6, p. 197, Jun. 2021, doi: 10.3390/photonics8060197.

[88] A. T. Pereda, F. Caminita, E. Martini, I. Ederra, J. Teniente, J. C. Iriarte, R. Gonzalo, and S. Maci, "Experimental validation of a Ku-band dual-circularly polarized metasurface antenna," *IEEE Trans. Antennas Propag.*, vol. 66, no. 3, pp. 1153–1159, Mar. 2018, doi: 10.1109/TAP.2018.2794395.

[89] A. H. Dorrah and G. V. Eleftheriades, "Two-dimensional center-fed transmission-line-grid antenna for highly efficient broadside radiation," *Phys. Rev. Appl.*, vol. 10, no. 2, Aug. 2018, Art. no. 024024, doi: 10.1103/physrevapplied.10.024024.

[90] Y.-H. Lv, Z. N. Chen, R. Wang, and B.-Z. Wang, "Dual-polarized multiresonant metantenna for quasi-independent radiation and in-band scattering manipulation," *IEEE Trans. Antennas Propag.*, vol. 71, no. 7, pp. 5895–5908, Jul. 2023, doi: 10.1109/TAP.2023.3281059.

[91] Y. Hu, X. Wang, X. Luo, X. Ou, L. Li, Y. Chen, P. Yang, S. Wang, and H. Duan, "All-dielectric metasurfaces for polarization manipulation: Principles and emerging applications," *Nanophotonics*, vol. 9, no. 12, pp. 3755–3780, Sep. 2020, doi: 10.1515/nanoph-2020-0220.

[92] B. Yin and Y. Ma, "Broadband terahertz polarization converter with anomalous reflection based on phase gradient metasurface," *Opt. Commun.*, vol. 493, Aug. 2021, Art. no. 126996, doi: 10.1016/j.optcom.2021.126996.

[93] S.-Y. Wang, J.-D. Bi, W. Liu, W. Geyi, and S. Gao, "Polarization-insensitive cross-polarization converter," *IEEE Trans. Antennas Propag.*, vol. 69, no. 8, pp. 4670–4680, Aug. 2021, doi: 10.1109/TAP.2021.3060087.

[94] W. Yang, K. Chen, X. Luo, K. Qu, J. Zhao, T. Jiang, and Y. Feng, "Polarization-selective bifunctional metasurface for high-efficiency millimeter-wave folded transmitarray antenna with circular polarization," *IEEE Trans. Antennas Propag.*, vol. 70, no. 9, pp. 8184–8194, Sep. 2022, doi: 10.1109/TAP.2022.3168746.

[95] C. X. Huang, J. Zhang, Q. Cheng, and T. J. Cui, "Polarization modulation for wireless communications based on metasurfaces," *Adv. Funct. Mater.*, vol. 31, no. 36, Sep. 2021, Art. no. 2103379, doi: 10.1002/adfm.202103379.

[96] Q. Ma, Q. R. Hong, X. X. Gao, H. B. Jing, C. Liu, G. D. Bai, Q. Cheng, and T. J. Cui, "Smart sensing metasurface with self-defined functions in dual polarizations," *Nanophotonics*, vol. 9, no. 10, pp. 3271–3278, Aug. 2020, doi: 10.1515/nanoph-2020-0052.

[97] J. He, Q. Zhu, Y. Zhou, J. Wang, G. Cai, M. Li, and J. Dong, "Lightweight switchable bifunctional metasurface based on VO_2: High-efficiency absorption and ultra-wideband circular polarization conversion," *Optik*, vol. 257, May 2022, Art. no. 168837, doi: 10.1016/j.ijleo.2022.168837.

[98] S. Sui, H. Ma, J. Wang, M. Feng, Y. Pang, J. Zhang, Z. Xu, and S. Qu, "Synthetic design for a microwave absorber and antireflection to achieve wideband scattering reduction," *J. Phys. D, Appl. Phys.*, vol. 52, no. 3, Nov. 2018, Art. no. 035103, doi: 10.1088/1361-6463/aaeb12.

[99] M. Feng, Y. Li, Q. Zheng, J. Zhang, Y. Han, J. Wang, H. Chen, S. Sai, H. Ma, and S. Qu, "Two-dimensional coding phase gradient metasurface for RCS reduction," *J. Phys. D, Appl. Phys.*, vol. 51, no. 37, Aug. 2018, Art. no. 375103, doi: 10.1088/1361-6463/aad5ad.

[100] X. Fu, J. Wang, Y. Fan, M. Feng, M. Yan, Y. Li, H. Chen, J. Zhang, and S. Qu, "Merging bands of polarization convertors by suppressing Fano resonance," *Appl. Phys. Lett.*, vol. 113, no. 10, Sep. 2018, Art. no. 101901, doi: 10.1063/1.5048247.

[101] Y. Fan, J. Wang, Y. Li, J. Zhang, Y. Han, and S. Qu, "Low-RCS and high-gain circularly polarized metasurface antenna," *IEEE Trans. Antennas Propag.*, vol. 67, no. 12, pp. 7197–7203, Dec. 2019, doi: 10.1109/TAP.2019.2920355.

[102] S. Sui, H. Ma, J. Wang, Y. Pang, M. Feng, Z. Xu, and S. Qu, "Absorptive coding metasurface for further radar cross section reduction," *J. Phys. D, Appl. Phys.*, vol. 51, no. 6, Jan. 2018, Art. no. 065603, doi: 10.1088/1361-6463/aaa3be.

[103] Y. Li, J. Wang, J. Zhang, S. Qu, Y. Pang, L. Zheng, M. Yan, Z. Xu, and A. Zhang, "Ultra-wide-band microwave composite absorbers based on phase gradient metasurfaces," *Prog. Electromagn. Res. M*, vol. 40, pp. 9–18, 2014, doi: 10.2528/pierm14092502.

[104] Y. Zhao, X. Cao, J. Gao, L. Xu, X. Liu, and L. Cong, "Broadband low-RCS circularly polarized array using metasurface-based element," *IEEE Antennas Wireless Propag. Lett.*, vol. 16, pp. 1836–1839, 2017, doi: 10.1109/LAWP.2017.2682848.

[105] P. Yang, F. Yan, F. Yang, and T. Dong, "Microstrip phased-array in-band RCS reduction with a random element rotation technique," *IEEE Trans. Antennas Propag.*, vol. 64, no. 6, pp. 2513–2518, Jun. 2016, doi: 10.1109/TAP.2016.2543781.

[106] S.-M. Wang, J. Gao, X.-Y. Cao, Y.-J. Zheng, T. Li, J.-X. Lan, and L.-R. Ji-Di, "Design of multi-band metasurface antenna array with low RCS performance," *Chin. Phys. B*, vol. 27, no. 10, Oct. 2018, Art. no. 104102, doi: 10.1088/1674-1056/27/10/104102.

[107] Z. Jiakai, Y. Yabing, W. Anqi, and Z. Jiaocheng, "A low RCS microstrip antenna based on a composite technology of slotting and loading split-rings," *Int. J. RF Microw. Comput.-Aided Eng.*, vol. 32, no. 11, p. 23361, Nov. 2022, doi: 10.1002/mmce.23361.

[108] Z. Li, W. Cui, R. Liu, K. Zhang, W. Liang, M. Wang, C. Fan, H. Zheng, and E. Li, "Investigation of leaky-wave antenna with stable wide beam-scanning characteristic," *IEEE Trans. Antennas Propag.*, vol. 70, no. 1, pp. 240–249, Jan. 2022, doi: 10.1109/TAP.2021.3111486.

[109] G. Xu, A. Overvig, Y. Kasahara, E. Martini, S. Maci, and A. Alù, "Arbitrary aperture synthesis with nonlocal leaky-wave metasurface antennas," *Nature Commun.*, vol. 14, no. 1, Jul. 2023, Art. no. 1, doi: 10.1038/s41467-023-39818-2.

[110] F. Mesa, G. Valerio, R. Rodríguez-Berral, and O. Quevedo-Teruel, "Simulation-assisted efficient computation of the dispersion diagram of periodic structures: A comprehensive overview with applications to filters, leaky-wave antennas and metasurfaces," *IEEE Antennas Propag. Mag.*, vol. 63, no. 5, pp. 33–45, Oct. 2021, doi: 10.1109/MAP.2020.3003210.

[111] A. Mehdipour, J. W. Wong, and G. V. Eleftheriades, "Beam-squinting reduction of leaky-wave antennas using Huygens metasurfaces," *IEEE Trans. Antennas Propag.*, vol. 63, no. 3, pp. 978–992, Mar. 2015, doi: 10.1109/TAP.2015.2389240.

[112] W. E. I. Liu, Z. N. Chen, and X. Qing, "Broadband low-profile L-probe fed metasurface antenna with TM leaky wave and TE surface wave resonances," *IEEE Trans. Antennas Propag.*, vol. 68, no. 3, pp. 1348–1355, Mar. 2020, doi: 10.1109/TAP.2019.2955629.

[113] N. Hussain, K. E. Kedze, and I. Park, "Performance of a planar leaky-wave slit antenna for different values of substrate thickness," *J. Electromagn. Eng. Sci.*, vol. 17, no. 4, pp. 202–207, Oct. 2017, doi: 10.26866/jees.2017.17.4.202.

[114] W. Fuscaldo, S. Tofani, D. C. Zografopoulos, P. Baccarelli, P. Burghignoli, R. Beccherelli, and A. Galli, "Systematic design of THz leaky-wave antennas based on homogenized metasurfaces," *IEEE Trans. Antennas Propag.*, vol. 66, no. 3, pp. 1169–1178, Mar. 2018, doi: 10.1109/TAP.2018.2794393.

[115] E. Abdo-Sánchez, M. Chen, A. Epstein, and G. V. Eleftheriades, "A leaky-wave antenna with controlled radiation using a bian-isotropic Huygens' metasurface," *IEEE Trans. Antennas Propag.*, vol. 67, no. 1, pp. 108–120, Jan. 2019, doi: 10.1109/TAP.2018.2878082.

[116] H. Huang and H. Wen, "Miniaturized reconfigurable tri-polarization metantenna based on characteristic mode analysis with high-aperture efficiency," *Int. J. RF Microw. Comput.-Aided Eng.*, vol. 31, no. 11, Nov. 2021, Art. no. e22867, doi: 10.1002/mmce.22867.

[117] Z. N. Chen, Q. Lou, and W. Liu, "Metantennas: Opportunities and challenges in future microwave metasurface antenna research and applications," in *Proc. 16th Eur. Conf. Antennas Propag. (EuCAP)*, Mar. 2022, pp. 1–5, doi: 10.23919/EuCAP53622.2022.9768992.

[118] P. Zhang, X. Zhang, and L. Li, "An optically transparent metantenna for RF wireless energy harvesting," *IEEE Trans. Antennas Propag.*, vol. 70, no. 4, pp. 2550–2560, Apr. 2022, doi: 10.1109/TAP.2021.3137166.

[119] Y.-H. Lv, R. Wang, B.-Z. Wang, and Z. N. Chen, "Anisotropic complementary metantenna for low sidelobe radiation and low in-band co-polarized scattering using characteristic mode analysis," *IEEE Trans. Antennas Propag.*, vol. 70, no. 11, pp. 10177–10186, Nov. 2022, doi: 10.1109/TAP.2022.3191138.

[120] Z. N. Chen, X. Qing, X. Tang, W. E. I. Liu, and R. Xu, "Phased array metantennas for satellite communications," *IEEE Commun. Mag.*, vol. 60, no. 1, pp. 46–50, Jan. 2022, doi: 10.1109/MCOM.001.2100538.

[121] F. A. Dicandia and S. Genovesi, "Characteristic modes analysis of non-uniform metasurface superstrate for nanosatellite antenna design," *IEEE Access*, vol. 8, pp. 176050–176061, 2020, doi: 10.1109/ACCESS.2020.3027251.

[122] P. Wang and Z. Shen, "End-fire surface wave antenna with metasurface coating," *IEEE Access*, vol. 6, pp. 23778–23785, 2018, doi: 10.1109/ACCESS.2018.2827199.

[123] J. Tao, X. Li, Y. Li, F. Teng, and H. Wu, "SIW-fed double layer end-fire metasurface antenna array with improved gain," in *Proc. Cross Strait Quad-Regional Radio Sci. Wireless Technol. Conf.*, Jul. 2019, pp. 1–3, doi: 10.1109/CSQRWC.2019.8799107.

[124] M. Bosiljevac, M. Casaletti, F. Caminita, Z. Sipus, and S. Maci, "Non-uniform metasurface Luneburg lens antenna design," *IEEE Trans. Antennas Propag.*, vol. 60, no. 9, pp. 4065–4073, Sep. 2012, doi: 10.1109/TAP.2012.2207047.

[125] X. Wan, X. Shen, Y. Luo, and T. J. Cui, "Planar bifunctional Luneburg-fisheye lens made of an anisotropic metasurface," *Laser Photon. Rev.*, vol. 8, no. 5, pp. 757–765, Sep. 2014, doi: 10.1002/lpor.201400023.

[126] A. Dhouibi, S. N. Burokur, and A. de Lustrac, "Planar metamaterial-based beam-scanning broadband microwave antenna," *J. Appl. Phys.*, vol. 115, no. 19, May 2014, Art. no. 194901, doi: 10.1063/1.4876233.

[127] F. Costa, A. Monorchio, and G. Manara, "An overview of equivalent circuit modeling techniques of frequency selective surfaces and metasurfaces," *Appl. Comput. Electromagn. Soc. J.*, vol. 29, no. 12, pp. 960–976, Dec. 2014.

[128] D. Sievenpiper, L. Zhang, R. F. J. Broas, N. G. Alexopolous, and E. Yablonovitch, "High-impedance electromagnetic surfaces with a forbidden frequency band," *IEEE Trans. Microw. Theory Techn.*, vol. 47, no. 11, pp. 2059–2074, Nov. 1999, doi: 10.1109/22.798001.

[129] C. Pfeiffer and A. Grbic, "Metamaterial Huygens' surfaces: Tailoring wave fronts with reflectionless sheets," *Phys. Rev. Lett.*, vol. 110, no. 19, 2013, Art. no. 197401, doi: 10.1103/physrevlett.110.197401.

[130] N. Yu and F. Capasso, "Flat optics with designer metasurfaces," *Nature Mater.*, vol. 13, no. 2, pp. 139–150, Feb. 2014, doi: 10.1038/nmat3839.

[131] Z. Bomzon, G. Biener, V. Kleiner, and E. Hasman, "Space-variant Pancharatnam-Berry phase optical elements with computer-generated subwavelength gratings," *Opt. Lett.*, vol. 27, no. 13, pp. 1141–1143, Jul. 2002, doi: 10.1364/ol.27.001141.

[132] V. Asadchy, M. Albooyeh, S. Tcvetkova, A. Díaz-Rubio, Y. Ra'di, and S. Tretyakov, "Perfect control of reflection and refraction using spatially dispersive metasurfaces," *Phys. Rev. B, Condens. Matter*, vol. 94, no. 7, 2016, Art. no. 075142, doi: 10.1103/physrevb.94.075142.

[133] N. I. Landy, S. Sajuyigbe, J. J. Mock, D. R. Smith, and W. J. Padilla, "Perfect metamaterial absorber," *Phys. Rev. Lett.*, vol. 100, no. 20, May 2008, doi: 10.1103/physrevlett.100.207402.

[134] G. Minatti, E. Martini, F. Caminita, S. C. Pavone, M. Albani, G. Toso, and S. Maci, "Electronically reconfigurable metasurface antennas based on liquid crystal technology," in *Proc. 13th Eur. Conf. Antennas Propag. (EuCAP)*, Mar. 2019, pp. 1–3. Accessed: Jan. 23, 2025. [Online]. Available: https://ieeexplore.ieee.org/document/8739310

[135] D. C. Zografopoulos, A. Ferraro, and R. Beccherelli, "Liquid-crystal high-frequency microwave technology: Materials and characterization," *Adv. Mater. Technol.*, vol. 4, no. 2, Feb. 2019, Art. no. 1800447, doi: 10.1002/admt.201800447.

[136] S. Foo, "Liquid-crystal-tunable metasurface antennas," in *Proc. 11th Eur. Conf. Antennas Propag. (EUCAP)*, Mar. 2017, pp. 3026–3030, doi: 10.23919/EuCAP.2017.7928122.

[137] X. Y. Wu, H. Y. Feng, F. Wan, M. Wei, C. Guo, L. Cai, F. Wu, Z. H. Jiang, L. Kang, W. Hong, and D. H. Werner, "An ultrathin, fast-response, large-scale liquid-crystal-facilitated multi-functional reconfigurable metasurface for comprehensive wavefront modulation," *Adv. Mater.*, vol. 36, no. 26, Jun. 2024, Art. no. 2402170, doi: 10.1002/adma.202402170.

[138] S. Ma, X.-N. Li, Z.-D. Li, and J.-J. Ding, "Electronic beam steering metamaterial antenna with dual-tuned mode of liquid crystal material," *Sensors*, vol. 23, no. 5, p. 2556, Feb. 2023, doi: 10.3390/s23052556.

[139] T. Qian, "Reconfigurable metasurface antenna based on the liquid metal for flexible scattering fields manipulation," *Micromachines*, vol. 12, no. 3, p. 243, Feb. 2021, doi: 10.3390/mi12030243.

[140] Y.-G. Park, H. S. An, J.-Y. Kim, and J.-U. Park, "High-resolution, reconfigurable printing of liquid metals with three-dimensional structures," *Sci. Adv.*, vol. 5, no. 6, p. 2844, Jun. 2019, doi: 10.1126/sciadv.aaw2844.

[141] *NASA 3D-Printed Antenna Takes Additive Manufacturing to New Heights—NASA*. Accessed: Jan. 31, 2025. [Online]. Available: https://www.nasa.gov/technology/nasa-3d-printed-antenna-takes-additive-manufacturing-to-new-heights/

MD ASHIF ISLAM ONI (Graduate Student Member, IEEE) received the B.Sc. and M.Sc. degrees (summa cum laude) in electrical and electronic engineering from American International University-Bangladesh (AIUB), Dhaka, Bangladesh, in February 2014 and February 2015, respectively, and the Erasmus Mundus Joint master's degree, in France and Spain, in December 2018. He is currently pursuing the Ph.D. degree with the Department of Electrical and Computer Engineering, North Dakota State University, Fargo, ND, USA.

He was a Lecturer and an Assistant Professor with the Department of Electrical and Electronic Engineering, AIUB, from September 2019 to December 2021. He had the opportunity to conduct research with Nokia Bell Labs, France, as a Research Intern, in 2018, as part of his Erasmus Mundus master's degree. Before getting the Erasmus Mundus scholarship from European Commission, he worked as a Lecturer with the Department of Electrical and Electronic Engineering, World University of Bangladesh (WUB), from August 2015 to August 2016. His research interests include metamaterials and metasurfaces for 5G and beyond, the Internet of Things, phased array antenna, satellite communications, RFID, next-generation fiber optic communication, and nano-photonics.

Mr. Oni was one of the two students who had been nominated for the Chancellor's award from the Department of Electrical and Electronic Engineering for their excellence in master's thesis research and outstanding academic results in the 15th convocation ceremony of AIUB.

YANG YANG (Senior Member, IEEE) was born in Bayan Nur, Inner Mongolia, China. He received the Ph.D. degree in electronic engineering from the Department of Electrical and Computer Systems Engineering, Monash University, Clayton, Australia, in 2013.

In 2012, he joined Rain Bird Australia, Melbourne, Australia, as an Asia Pacific GSP Engineer. In April 2015, he returned to academia, holding the position of a Senior Research Associate in microwave and antenna technologies with Macquarie University. In April 2016, he was appointed as a Research Fellow with the State Key Laboratory of Terahertz and Millimeter Waves, City University of Hong Kong. In December 2016, he joined the University of Technology Sydney (UTS), Australia. He is currently a Professor and a Group Leader of 3D Millimetre-Wave and Terahertz Circuits and Antennas with UTS Tech Lab. He has over 300 international publications in microwave, millimetre-wave, and terahertz circuits and antennas. His research interests include additively manufactured electronics, millimetre-wave and sub-terahertz technologies in 5G and beyond, and biomedical applications.

Dr. Yang was a Committee Member of the AP-S Technical Committee on Antenna Measurements and the AP-S Technical Directions Committee, from 2022 to 2024. He was a Australian Research Council Mid-Career Industry Fellow, from 2025 to 2029. He is a Committee Member of IEEE AP-S TC-8 Wireless Communication and IEEE MTT-S TC-28 Biological Effects and Medical Applications. He was selected as one of the ''Top 2 % Most Highly Cited Scientists by Stanford'' every year, since 2019. He received many distinguished awards, including the 2025 Advanced Materials Innovation Award by the International Association of Advanced Materials (IAAM), the 2024 IEEE MTT-S IMS First Place in the Early Career Award Competition (serving as the ECR Advisor), the 2023 IEEE NSW Section Outstanding Service Award, the 2023 IEEE AP-S Outstanding Chapter Award, and the 2022 IEEE MTT-S Outstanding Chapter Award. He is the Inaugural Chair of the IEEE MTT-S TC-17 Microwave Materials and Processing Technologies. His appointments at the IEEE NSW Section, Region 10, include a Committee Member of the IEEE NSW Section, the Treasurer and the Chair/Vice Chair of the IEEE NSW AP/MTT Joint Chapter, from 2018 to 2019 and from 2020 to 2024, respectively, the Secretary of IEEE NSW PH/ED/SSC/CAS Joint Chapter, in 2019, the Inaugural Committee/Treasurer, in 2020, and the Vice Chair of IEEE NSW Electron Devices Chapter, from 2022 to 2024. He also volunteered in various conference organizing committees, such as the General Co-Chair of the 2025 Australian Microwave Symposium, General Co-Chair (Executive Chair) of the inaugural annual international conference on IEEE Additively Manufactured Electronic Systems (AMES2025), and the General Chair of IEEE MTT-S International Microwave Workshop Series on Advanced Materials and Processes for RF and THz Applications (IMWS-AMP 2026). He is an Associate Editor of IEEE TRANSACTIONS ON MICROWAVE THEORY AND TECHNIQUES, in October 2022, and IEEE MICROWAVE AND WIRELESS TECHNOLOGY LETTERS, in October 2024, a Guest Editor of Proceedings of IEEE (2024), an Associate Editor of IEEE ACCESS, from 2018 to 2022, an Area Editor of *Microwave and Optical Technology Letters*, from 2019 to 2024, and a Guest Editor of IEEE ANTENNAS AND WIRELESS PROPAGATION LETTERS, in 2022.

SHUVASHIS DEY (Member, IEEE) received the Bachelor of Technology (B.Tech.) degree in electronics and communication engineering from National Institute of Technology-Durgapur, West Bengal, India, in 2007, the M.Sc. degree in wireless networks (physical pathway) from Queen Mary University of London, England, U.K., in 2009, and the Ph.D. degree in electrical and computer systems engineering from Monash University, Australia, in 2018.

He was a Research Affiliate with the Auto-ID Labs, Massachusetts Institute of Technology (MIT), Cambridge, USA, from 2016 to 2020. He was also a Post-doctoral Research Fellow with the Department of Electrical and Computer Systems Engineering, Monash University, from 2019 to 2021. He is currently an Assistant Professor with the Department of Electrical and Computer Engineering, North Dakota State University. His research interests include microwave devices and antennas, wearable antennas for healthcare applications, metamaterials and metasurfaces, as well as RFID tags and sensors.

Dr. Dey's awards and honors include the Young Scientist's Travel Grant at the IEEE International Symposium on Antennas and Propagation (ISAP) 2012, the IEEE MTT-S Ph.D. Student Sponsorship Initiative Award, in 2016, and the Best Presentation Award at the International Conference on Sensing Technology (ICST) 2017.